

Vibration Control Analysis of Aircraft Wing by Using Smart Material

Hussein Abdulridha Abdulameer Dr. Hatem R. Wasmi

Department of Mechanical Engineering, College of Engineering, University of Baghdad, Iraq

Abstract

Many of the mechanical systems exposed to undesired vibrations. These vibrations are removed by using active vibration control (AVC) and hence stability the response of the system. Smart structure technology is used for vibration reduction. Therefore the aircraft wing is embedded by Piezoelectric as a sensor and actuator. This material has fast response times and generates large amounts of force. Active vibration control was achieved by used output feedback control. An aircraft wing is numerically modelled with a used shell element and a couple filed analysis on piezoelectric between the displacement and the voltage. Output feedback control has been inserted to a finite element method by using ANSYS parametric design language (APDL). The control of free and forced vibration for smart structure was investigated. Free vibration is produced by aerodynamic force (lift force) at maximum speed of the aircraft and by the initial condition. Harmonic excitation (sin wave) is considered in the forced vibration control by using a piezoelectric shaker. Active vibration control was studied with different control gains and actuation voltages which affected the vibration control. The effect of changing the position of PZT, collected pair on mass and stiffness of smart structure as passive control (Control OFF) was investigated and then the optimal location was found. Experimental works for active vibration control of smart structure have been presented to verify the closed loop simulations. Free vibration, force vibration and natural frequency are obtained for experimental works by LABVIEW programs. It was observed that APDL ANSYS results were well matched with the experimental results. Settling time for free vibration, when the control OFF, is 15s, and when the control ON it is 3s. Displacement Amplitude for force vibration when the control is OFF it is $\pm 0.04\text{m}$ and when the control is ON it is $\pm 0.0005\text{m}$.

Keywords: Smart material, Aircraft wing, Active vibration control.

1. Introduction

The basic functions of an aircraft wing structure are to transmit and resist the applied loads. It consists of thin shell structures supported by longitudinal stiffening members and transverse frames to enable it to resist bending, compressive and torsional loads. In spite of this strong structure, the undesired vibration is generated because of the aerodynamic effect. This makes it able to model lighter mechanical systems withstand higher mechanical loads at higher speeds without any vibration. Smart materials and active control methods can be used to remove the undesired vibration by automatic modification of the system's structural response or controlled by applying counter force that is reverse to original force but equal in amplitude to the original vibration to achieve the desired response. As a result two opposite force cancel each other and structure becomes stable. The system mainly requires actuators, sensors and control mechanism that performs well when vibration occurs. Active vibration control finds its application in all the modern day machines, Engineering structures, bridges, trusses, buildings, mechanical systems, automobiles, electronics etc. As it needs only a little actuation voltage hence it does not requires any external power source, the power can be directly derived from the host machine itself. As the electronics is also developing at a very fast rate hence the size of a processor is also reducing, which is very useful in the design of the control system.

2. Aircraft Wing Structure

The airfoil type is HQ 3.5/10. This airfoil has been designed by Helmut Quabeck. The total wing span measures 5m so the spars are the most important structural component of the wings. Merlo's wing has a total of four spars: a main central spar, a front spar, a back spar and the spar at which the control surface, the flap, is attached. The first two spars, the main and the front, are expected to carry most of the load. They are built in the same way, being the front one a smaller version of the main spar. The spar consist of two beams made of fir wood that run all the way from the aircraft plane of symmetry to the rib located at 1.8m from the effective wing root. The total length of the main spar is 2.1m, including 300mm from the plane of symmetry of the aircraft to the beginning of the wing. The beams of the main spar are tapered from a width of 100mm at the intersection with the fuselage to a width of 50mm at the last rib. The front spar has two constant-width beams of 30mm. The ribs are placed perpendicularly to the wooden beams at a constant interval of 150mm. Thus, in the main part of the wing are allocated $1800/150 = 12$ ribs, plus one at the beginning, making a total of 13 ribs without the ribs for wing tip. Between the ribs, two vertical side beams made of birch plywood are glued to the main beams. The horizontal beams plus the side plates make a sort of hollow-rectangular cross-section. The height of the cross-section is not indicated since it must match the thickness of the airfoil at each section. For this reason the spars result to be

slightly tapered also in the vertical direction. Referring to the effective root airfoil, the center of the main spar is located at 320mm from the leading edge, while the front is located at 100mm from the leading edge. The last two spars are made of carbon rovings, with a constant hollow-circular cross section of diameter 20mm. The thickness is assumed to be of 0.8mm. The back spar cross-section center is located at approximately 540mm from the leading edge at the first rib. The back spar is placed perpendicularly with respect to the rib plane. The flap spar is located approximately at 12% of the airfoil chord from the trailing edge, resulting inclined relatively to the ribs. The ribs are cut between the back and the flap spar, leaving enough room for a $\pm 45^\circ$ rotation of the flap. The wing tip skin is sustained by a total of three ribs. The first is located at 100mm from the wing end, the middle at 150mm from the first one and the last at the tip end therefore the total number of ribs including tip wing is sixteen. The wing tip will be connected to the main wing with a carbon-carbon tube as the ones used for the back and flap spars. The tube is placed into the main spar, starting from the 9th rib and going into the tip, ending at the middle tip rib and called front spar tip. The first tip rib is also connected with a 12mm aluminum axle to the back spar and called back spar tip. [1] The wing structure is shown in the Figure 1.

3. Aircraft wing materials

The wing skin material selection is fundamental due to the skin function. The skins have been modelled using various layers of glass fiber in epoxy matrix. This material presents an orthotropic behaviour is made of 9 layers of glass fiber in epoxy matrix. The layers have been placed respectively at $[0/-45/+45/90/0/90/+45/-45/0]$ as shown in the Figures 2. Wood is still an excellent material for the construction of light aircrafts due to its good strength-to-weight ratio & long fatigue life, longer than aluminium or steel. Wood mechanical behaviour is typically orthotropic: it has different properties (Modulus of elasticity, strength etc.) in the direction of three perpendicular axes. Based on the foregoing above the material chose for main & front spars are silver fir wood and birch plywood for each spar. They are built in the same way, the spar consist of two horizontal beams made of silver fir wood. Between the ribs, two vertical side beams made of birch plywood are glued to the main beams. The birch plywood, also called aircraft plywood, is widely used in the construction of aircraft models. In fact, it is obtained by gluing with resin very thin birch veneers at high temperature and pressure. In this way, all the defects are discarded, and the hardened resin adds resistance to the material, making the compression strength almost equal to the tension, and reducing the anisotropic effect. The thickness of birch plywood is 1.2mm, made of three 0.4mm layers. The layers have been placed respectively at $[0/90/0]$ as shown in the Figure 3. The thicknesses of silver fir wood beams are five different thicknesses have been used, respectively of 5, 10, 15, 20 and 25mm. The different sections defined for the fir beams have been associated to different areas. The thickest section of 25mm has been associated to areas located from the beginning of the spar to the second rib, for a total length of $300 + 150 = 450$ mm. The section of 20mm thickness has been associated with areas from the second to the third spar, the one of 15mm thickness with areas from the third to the fourth and the one of 10mm thickness with areas from the fourth to the seventh. The remaining part of the fir beam has been associated with the section of 5mm thickness. Figure 4 shows the variation of thickness at the different ribs. For the back and flap spars of the wing chose carbon-carbon pipes (carbon fiber in carbon (epoxy) matrix) to get highly resistant, light and space-saving beams. Carbon-carbon may be considered an isotropic material. The ribs are made of 10mm thick flex foam sheets (M-130). Flex foam is an expanded closed cell PVC. It is good rigidity and strength-to-weight ratio. Mechanical properties are shown in table 1.

4. Wing Specification

The specifications of smart aircraft wing which used in this paper are shown in table 2 and figure 5.

5. Finite Element Method

Finite element modeling for smart aircraft wing is presented to evaluate the stiffness, mass and damping matrix of the mechanical system. After obtain the mathematical modeling for free & force vibration, i.e. the set of partial differential equations (Equations of Motion) and boundary conditions, has been numerically solve by using the Mechanical APDL (ANSYS) program to evaluate the natural frequency, mode shape, free vibration response with or without control and force vibration response with or without control. The finite element method must be used to solve the problem due to the complexity of the smart wing structure and boundary conditions. A precise mathematical model is required for the controller design for vibration control to predict the structure's response.

5.1 Stiffness Matrix $[k]_e$ for Shell Element

The stiffness matrix could be obtained from calculating the strain energy U . Applying the principle of variation approach [2], the strain energy for the element may be written as:

$$U = \frac{1}{2} \iiint_V (\bar{\varepsilon}_e^T \bar{\sigma}_e) dV \quad (1)$$

Where:

$$\bar{\epsilon} = [B]\bar{\delta} \quad (2)$$

$$\bar{\sigma}' = [D']\bar{\epsilon}' \quad (3)$$

Substituting equations (2) and (3) in equation (1) yields,

$$U = \frac{1}{2}\bar{\delta}_e^T \left[\iiint_V [B]^T [D][B] dV \right] \bar{\delta}_e \quad (4)$$

Or

$$U = \frac{1}{2}\bar{\delta}_e^T [K]_e \bar{\delta}_e \quad (5)$$

Where, $[K]_e$ is the element stiffness matrix and takes the form;

$$[K]_e = \iiint_V [B]^T [D][B] dV \quad (6)$$

5.2 Consistent Mass Matrix $[M]_e$ for Shell Element

The mass matrix $[M]_e$ might be obtained by calculation the kinetic energy KE [2], and can be written as:

$$KE = \frac{1}{2}\bar{\delta}_e^T \left[\rho \iiint_V [N]^T [N] dV \right] \bar{\delta}_e \quad (7)$$

Or,

$$KE = \frac{1}{2}\bar{\delta}_e^T [M]_e \bar{\delta}_e \quad (8)$$

Where, $[M]_e$ is the consistent mass matrix and is defined as:

$$[M]_e = \rho \iiint_V [N]^T [N] dV \quad (9)$$

Where, $[N]$ is the shape function matrix.

5.3 Equation of Motion for Finite Element

The equation of motion (or dynamic equation) can be derived, using the energy balance principle which involves that "the summation of the structure energies is stationary", i.e., the summation of kinetic energy, dissipation energy, strain energy and potential energy is stationary, or

$$KE + DE + U + PE = \text{Stationary} \quad (10)$$

If these energies are defined in terms of a nodal displacement vector $\bar{\delta}$, then,

$$\frac{\partial}{\partial \bar{\delta}} (KE + DE + U + PE) = 0 \quad (11)$$

The potential energy PE (with the absence of body forces) can be written as:

$$PE = -W = -\bar{\delta}_e^T \bar{F}_e(t) \quad (12)$$

Where, $\bar{F}_e(t)$ is the nodal forces vector.

Substituting equations (5), (8), and (12) in equation (11) gives,

$$\frac{\partial}{\partial \bar{\delta}_e} \left(\frac{1}{2}\bar{\delta}_e^T [M]_e \bar{\delta}_e + \frac{1}{2}\bar{\delta}_e^T [C]_e \bar{\delta}_e + \frac{1}{2}\bar{\delta}_e^T [K]_e \bar{\delta}_e - \frac{1}{2}\bar{\delta}_e^T \bar{F}_e(t) \right) = 0 \quad (13)$$

The derivation of the first term of the upper equation is obtained as follows:

$$\frac{\partial}{\partial \bar{\delta}_e} \left(\frac{1}{2}\bar{\delta}_e^T [M]_e \bar{\delta}_e \right) = \frac{d}{dt} \frac{\partial \bar{\delta}_e}{\partial \bar{\delta}_e} \frac{\partial}{\partial \bar{\delta}_e} \left(\frac{1}{2}\bar{\delta}_e^T [M]_e \bar{\delta}_e \right) = \frac{d}{dt} ([M]_e \bar{\delta}_e) = [M]_e \dot{\bar{\delta}}_e$$

The other terms can be easily derived to get the final form of the dynamic equation of finite element.

$$[M]_e \dot{\bar{\delta}}_e + [C]_e \bar{\delta}_e + [K]_e \bar{\delta}_e = \bar{F}_e(t) \quad (14)$$

$$[C] = \alpha * [M] + \beta * [K] \quad (15)$$

Where α and β are the structural damping constant

6. Piezoelectric Equations

The unstressed in one dimensional dielectric medium, the displacement of electric D (charge per unit area C/m²) is related to the field of electric E (V/m) by.

$$D = e E \quad (16)$$

Where:

e = dielectric constant of the Piezoelectric

As well as in one dimensional elastic body placed in zero field of electric, the stress T (N/m²) and the strain S are related by

$$S = s T \quad (17)$$

Where:

s = compliance of the Piezoelectric (inverse of the Young modulus).

For piezoelectric material, the mechanical and electrical constitutive equations are coupled.

$$S = s^E T + d E \quad (18)$$

$$D = d T + \epsilon^T E \quad (19)$$

Where in Equation (18):

d = piezoelectric constant relate the strain to the field of electric E in the absence of mechanical stresses.

s^E = the compliance when the electric field E is constant.

Where in Equation (19):

d relates the electric displacement D to the stress under zero field of electric E (m/V or Coulomb/Newton).

ϵ^T = dielectric constant under constant stress.

If the direction of the polarization synchronizes with direction 3 then constitutive equation for the sensing and actuation mechanisms can be rewritten in matrix form [3]:

Actuation:

$$\begin{Bmatrix} S_{11} \\ S_{22} \\ S_{33} \\ 2S_{23} \\ 2S_{13} \\ 2S_{12} \end{Bmatrix} = \underbrace{\begin{bmatrix} s_{11} & s_{12} & s_{13} & 0 & 0 & 0 \\ s_{12} & s_{22} & s_{23} & 0 & 0 & 0 \\ s_{13} & s_{23} & s_{33} & 0 & 0 & 0 \\ 0 & 0 & 0 & s_{44} & 0 & 0 \\ 0 & 0 & 0 & 0 & s_{55} & 0 \\ 0 & 0 & 0 & 0 & 0 & s_{66} \end{bmatrix}}_{\text{Compliance}} \begin{Bmatrix} T_{11} \\ T_{22} \\ T_{33} \\ T_{23} \\ T_{13} \\ T_{12} \end{Bmatrix} + \underbrace{\begin{bmatrix} 0 & 0 & d_{31} \\ 0 & 0 & d_{32} \\ 0 & 0 & d_{33} \\ 0 & d_{24} & 0 \\ d_{15} & 0 & 0 \\ 0 & 0 & 0 \end{bmatrix}}_{\text{Coupling}} \begin{Bmatrix} E_1 \\ E_2 \\ E_3 \end{Bmatrix} \quad (20)$$

Sensing:

$$\begin{Bmatrix} D_1 \\ D_2 \\ D_3 \end{Bmatrix} = \underbrace{\begin{bmatrix} 0 & 0 & 0 & 0 & d_{15} & 0 \\ 0 & 0 & 0 & d_{24} & 0 & 0 \\ d_{31} & d_{32} & d_{33} & 0 & 0 & 0 \end{bmatrix}}_{\text{Coupling}} \begin{Bmatrix} T_{11} \\ T_{22} \\ T_{33} \\ T_{23} \\ T_{13} \\ T_{12} \end{Bmatrix} + \underbrace{\begin{bmatrix} \epsilon_{11} & 0 & 0 \\ 0 & \epsilon_{22} & 0 \\ 0 & 0 & \epsilon_{33} \end{bmatrix}}_{\text{permittivity}} \begin{Bmatrix} E_1 \\ E_2 \\ E_3 \end{Bmatrix} \quad (21)$$

Examining actuator equation (20), when field of electric E3 is applied parallel to the direction of polarization, the extension is observed along same direction (direction of polarization) and its amplitude is controlled by the piezoelectric coefficient constant d33. Shrinkage is obtained along the direction one (1) and two (2) orthogonal to the electric field and its amplitude of which is governed by d31 and d32 respectively. Piezoceramic has an isotropic behaviour in the plane d31 = d32.

7. Finite Element Method for piezoelectric

Mechanical APDL (ANSYS) program offers three and two dimensional piezoelectric coupled field elements in order to modelling smart structures with piezoelectric sensors / actuators. Static, modal, transient analysis and full harmonic can be performed with this finite element program. They have the capability of modelling piezoelectric. Piezoelectric elements have four degree of freedom (DOF) at each node (ux, uy, uz and volt). In this case of vibration reduction, it is necessary use 'coupled-field analysis' to couple the interaction between electric field and applied stress therefore coupled field elements that consider electrical and structural coupling are required in order to perform the finite element analysis of smart structure. The coupled field element shall be containing all necessary nodal DOF.

7.1 Finite Element Formulation for Piezoelectric

Piezoelectricity is considered a linear theory in which the elastic, piezoelectric, and dielectric coefficients are treated as constants. Constitutive equations that Mechanical APDL (ANSYS) use to model piezoelectric material are rearranged in matrix form as the following [4].

$$\begin{Bmatrix} \{T\} \\ \{D\} \end{Bmatrix} = \begin{bmatrix} [c] & [e] \\ [e]^T & [-\epsilon] \end{bmatrix} \begin{Bmatrix} \{S\} \\ \{-E\} \end{Bmatrix} \quad (22)$$

Therefore, Mechanical APDL (ANSYS) only considers these material properties for piezoelectric three dimension elements, including elastic stiffness matrix or compliance matrix, piezoelectric matrix [e] or [d] and permittivity matrix.

For finite element piezoelectric, using shape functions and nodal solution variables can be obtain the displacements and electrical potentials for element domain:

$$\{u_c\} = [N^u]^T \{u\} \quad (23)$$

$$V_c = [N^V]^T \{V\} \quad (24)$$

Where

{uc} = displacements for element domain in x, y, z directions

Vc = electrical potential for element domain

[N^u] = displacement shape functions matrix

[N^v] = electrical potential shape function

{u} = nodal displacements vector

{V} = nodal electrical potential vector

Then the strain vector {S} and electric field vector {E} are related to the displacements and potentials respectively,

$$\{S\} = [B_u] \{u\} \quad (25)$$

$$\{E\} = - [B_v] \{V\} \quad (26)$$

Where:

$$[B_u] = \begin{bmatrix} \partial/\partial x & 0 & 0 \\ 0 & \partial/\partial y & 0 \\ 0 & 0 & \partial/\partial z \\ \partial/\partial y & \partial/\partial x & 0 \\ 0 & \partial/\partial z & \partial/\partial y \\ \partial/\partial z & 0 & \partial/\partial x \end{bmatrix} \quad (27)$$

$$[B_v] = \begin{bmatrix} \partial/\partial x \\ \partial/\partial y \\ \partial/\partial z \end{bmatrix} \{N^v\}^T \quad (28)$$

Mechanical response of piezoelectric elements can be expressed by the equation of motion [5]:

$$\{\text{div}[T]\} + \{f\} = \rho \{\ddot{u}\} \quad (29)$$

Where T, f, ρ and ü are stress, body force in unit volume, density and acceleration, respectively.

Electrical response of piezoelectric elements can be described by Maxwell's equation:

$$\{\partial D/\partial x\} = 0 \quad (30)$$

With the application of variational principles on the mechanical equilibrium equation, Equation (29) and the electrical flux conversation equation, Equation (30), in conjunction with the approximate field of equation (23, 24, 25, 26) and the constitutive properties in Equation (22), the piezoelectric finite element formulation can be derived in terms of nodal quantities:

$$\begin{bmatrix} [M] & [0] \\ [0] & [0] \end{bmatrix} \begin{Bmatrix} \{u\} \\ \{v\} \end{Bmatrix} + \begin{bmatrix} [C] & [0] \\ [0] & [0] \end{bmatrix} \begin{Bmatrix} \{u\} \\ \{v\} \end{Bmatrix} + \begin{bmatrix} [K] & [K^z] \\ [K^z]^T & [K^d] \end{bmatrix} \begin{Bmatrix} \{u\} \\ \{V\} \end{Bmatrix} = \begin{Bmatrix} \{F\} \\ \{L\} \end{Bmatrix} \quad (31)$$

Where:

[M] = mass matrix derived from density and volume

[K] = mechanical stiffness matrix derived from elastic matrix

[K^z] = piezoelectric stiffness matrix derived from piezoelectric matrix

[K^d] = dielectric stiffness matrix derived from dielectric matrix

{F} = mechanical force vector

{L} = charge vector

[M], [K], [K^z] and [K^d] matrices are expressed as:

$$\text{Structural mass matrix: } [M] = \int_V \rho [N^u][N^u]^T dv \quad (32)$$

$$\text{Structural stiffness matrix: } [K] = \int_V [B^u]^T c [B^u] dv \quad (33)$$

$$\text{Piezoelectric coupling matrix: } [k^z] = \int_V [B^u]^T e [B_v] dv \quad (34)$$

$$\text{Dielectric conductivity matrix: } [K^d] = \int_V [B_v]^T \epsilon [B_v] dv \quad (35)$$

Energy coefficients are calculated for each piezoelectric element as follows:

$$\text{Elastic energy: } U_E = 1/2 \{S\}^T [c] \{S\} \quad (36)$$

$$\text{Dielectric energy: } U_D = 1/2 \{E\}^T [\epsilon] \{E\} \quad (37)$$

$$\text{Electromechanical coupling energy: } U_M = - 1/2 \{S\}^T [e] \{E\} \quad (38)$$

$$\text{Potential energy: } E^P = U_E + U_D \quad (39)$$

8. Element Type of Smart Aircraft Wing in Mechanical APDL (ANSYS)

The smart wing of the aircraft consists of spars, ribs, skin and piezoelectric therefore the wing will be divided into elements for the isotropic, orthotropic and coupled field to perform the finite element analysis of smart structures. The number of mesh which used for smart wing is 11149 elements and for smart beam is 1872 elements.

8.1 SHELL181 Element Description:

SHELL181 is appropriate for analyzing thin to thick shell structure. It has translations in the x, y and z directions and rotations about the x, y, and z-axes therefore six degrees of freedom at each node and it is four node elements.

Change in shell thicknesses are accounted for analyses. SHELL181 can be used for layered applications for modeling composite shells or sandwich construction. The accuracy in modeling composite shells is governed by the first-order shear-deformation theory (usually referred to as Mindlin- eissner shell theory). The element formulation is based on logarithmic true stress and strain measures. [6]

8.2 SOLID5 Element Description:

SOLID5 has a 3-D magnetic, thermal, electric, piezoelectric and structural field capability with limited coupling between the fields. The element has 8 nodes. Each node has u_x , u_y and u_z displacements along x , y , and z axis, respectively. With up to 6 DOF at each node. When used in structural and piezoelectric analyses, SOLID5 has large deflection and stress stiffening capabilities. A prism shaped element is formed by defining duplicate node numbers. The prism shaped element may be useful in modeling a system that has a geometric curvature (e.g., cylinder). When chosen this type of piezoelectric, Mechanical APDL ANSYS will only consider the behaviors of SOLID5 in u_x , u_y , u_z and volt degrees of freedom. It should be noted that u_x , u_y and u_z indicate the displacements in the global coordinate system x , y and z directions, while volt indicates the difference in potential energy of the electrical particles between two locations. [6] The element type and boundary condition is shown in the figure 6.

9. Output Feedback Control (AVC)

Output feedback is a theory for closed-loop system for smart mechanical structures being controlled by position and or velocity feedback. The systems have the form as the following [7]

$$M\ddot{q}(t) + C\dot{q}(t) + Kq(t) = f_r + f(t) \quad (40)$$

Where, the vector $f(t)$ represents external disturbance forces (such as aerodynamic force) and the vector f_r represents the control force stem from the action of r force actuators and defined as the following

$$f_r = B_f U \quad (41)$$

Here, the $r \times 1$ vector u represents the r input, one for each control device (actuator). The matrix B_f represents the locations on the structure of any actuators or devices being used to supply the forces u . such as, electromechanical or piezoelectric actuator are attached to the structure. The feedback of the velocity and position, let y denoted $s \times 1$ vector of sensor outputs as the following

$$y(t) = C_p q(t) + C_v \dot{q}(t) \quad (42)$$

Here, C_p and C_v are $s \times n$ matrices of displacement and velocity influence coefficients, with structure obtained by the sensor locations and the electronic gains associated with the transducers used to measure the various state variables and here the s denotes the number of sensors. Equation (42) represents those coordinates which are measured as part of the active control system and is the mathematical model of the signal processing and transducer used to measure the structural response. In this paper taken the matrix C_v zero due to don't use velocity feedback. The special form of the input vector u is chosen as the following

$$U(t) = -G_f y(t) = -G_f C_p q(t) - G_f C_v \dot{q}(t) \quad (43)$$

Here the $r \times s$ matrix G_f consists of feedback constant gains. The form of control law (equation 43) is output feedback, due to the input is proportional to the measured output for the response y . If Equation (41) is substituted into Equation (40) to yield the closed-loop system as the following [8]:

$$M\ddot{q}(t) + C\dot{q}(t) + Kq(t) = B_f U(t) + f(t) \quad (44)$$

In this case, the control vector u is a function of the response coordinates of interest, denoted by the vector y , i.e. $U(t) = -G_f y$. Equations (42), (43) and (44) can be representation in the block diagram of Figure (7).

10. Active Vibration Control Simulation in Smart Structures

All of the analyses are performed with using mechanical APDL (ANSYS). Control action is inserted into the finite element model of multi degrees of freedom vibration system. Controls performance is estimated in the finite element environment describing the outputs and inputs of the system step by step. The reference of input value is taken as zero in the feedback (closed loop) vibration control system. The instantaneous value of the voltage (VS) (strain rate) for the sensor location at time step is subtracted from zero to obtain the error signal value. Error signal is the difference between the zero (input reference) and the sensor signal to obtain inverted signal for each time step to generate reverse force to the original vibration. The control gain (KC) and amplifier gain (KV) are multiplied by the error value to calculate the voltage value (VA) and used this voltage as the input to the actuator node at a time step. The value of the control gain (KC) is taken differently for obtain the best vibration control. The processes are continuous with the selected time step until the response is reached for steady-state value. The differential control action require smaller time step for higher precision. t_s is the settling time at which the steady state of response is reached. The natural frequencies of open-loop system are found for all piezoelectric location to compare the stiffness and the settling time of smart structure and hence selected the optimal location of piezoelectric as passive control.

10.1 Free Vibration due to Aerodynamic Force

The block diagram of the analysis for active vibration control in smart structures is shown in Figure 8. Free vibration is performed due to applied aerodynamic force (lift force) on the aerodynamic center of the smart aircraft wing at the analysis of the first time step (before beginning of closed loop system) and then give this force zero at beginning of closed loop system to obtain free vibration due to force. K_C & K_V are the control and power amplification factors, respectively. K_V is taken as 100 by inspection PZT amplifier gain. The voltage values (V_S) of the sensor location are taken as the feedback loop. The proportional control (K_C) is only applied. Thus, the proportional constant for the voltage of actuator (V_A) is the multiplication of $K_C * K_V$. The value of actuator voltage (V_A) is change in each time step corresponding to the voltage sensor (V_S) and the multifunction of K_C & K_V are constant in each time step. The calculated deflection U_Z is observed to evaluate the performance for the response of vibration control. Effective actuation and sensing of control action depend on the locations of actuators and sensors. The actuator and sensor locations are very important to obtain maximize actuator effective. The positions of the aircraft wing at the mechanical strain is maximum are the best location for actuators and sensors. The objectives of the control are to place all of the actuators and sensors in multi different areas. Modal analysis of the aircraft wing is required to design the locations of actuators and sensors.

10.2 Free Vibration due to Initial Displacement

Static analysis is performed by applying the Initial Displacement to the tip of the smart aircraft wing. All nodal displacements are obtained for the Initial Displacement of the tip and save these displacements in matrix form. Initial condition is describe using these nodal displacements for all nodes of the smart aircraft wing and then applied these displacements as initial condition (IC) to obtain free vibration. Initial Displacement at the tip of smart aircraft wing is obtaining approximately from applied the aerodynamic force in previous section. The block diagram of this analysis is shown in Figure 9.

10.3 Force Vibration due to PZT Shaker (Harmonic Excitation)

First mode of the vibration is considered in the feedback (closed loop) control analysis. Block diagram of the closed feedback (closed loop) is given in Figure 10. Force vibration is obtained from PZT shaker this shaker is programming to provide the smart structure harmonic excitation (Sine Wave) and then control this excitation by AVC. Control action is achieved with the script code after the finite element model of the smart aircraft wing with PZT shaker is constructed. Harmonic excitation is created in the finite element model before the feedback is beginning. Then, the first step is solved by applying the excitation voltage to the PZT shaker. Hence, the nodal solutions of the finite element model are known for the next step. The excitations are applied again in the first step of the feedback. The voltage known from the first step is read from PZT sensor location. Error signal is obtained after the voltage value is calculated. The actuation voltage (V_A) to be applied for the piezoelectric actuator is found by multiplying error signal by the gain K_C & K_V . Therefore, the analysis starts on step by step for a specific time after vibration amplitudes (response) reach steady-state.

11. Experimental Work

The experiments are conducted to verify the simulation results. Piezoelectric as actuator, sensor & shaker have been tested for active vibration control on cantilever aluminium beam type 7075 T6 which is used in aircraft manufacturing. First, modal analysis is done to find natural frequency. Second, free vibration of the beam under tip initial displacement is considered. In free vibration the aluminium smart beam is embedded of two piezoelectric (PZT) patches. One of the piezoelectric patches is used as controlling actuator while the other piezoelectric patch is used as vibration sensor. Third, the active control of a smart beam under forced vibration is considered. The aluminium smart beam is embedded of three piezoelectric patches. One of the piezoelectric patches is used as controlling actuator while the second piezoelectric patch is used as vibration sensor and the third piezoelectric patch is used as vibration generating shaker. The smart beam is harmonically excited by the piezoelectric shaker at its fundamental frequency. AVC for free vibration and under harmonic excitation was achieved using output feedback control. The signals for all cases are found experimentally and also by the simulation to compare the results between them. The experimental results are obtained by using Lab VIEW program. Control OFF and Control ON vibration signals are obtained for various gains. Dynamic behaviour at the tip of the beam is evaluated for the uncontrolled and controlled responses. Closed loop simulations for smart beam are performed by APDL also. The simulation and experimental results are compared. It is observed that the simulation results obtained by the finite element procedure are in good agreement with the experimental results.

12. Hardware Devices

The hardware devices for active vibration control are illustrated as the following

12.1 High Voltage Amplifier of PZT (HVPZT)

This device consists of three high-voltage amplifiers type PI Model E-507 that offer high performance and wide bandwidth, sensor and position servo control modules type E-509 and display modules for modular PZT controller type E-515. The output voltage is 1100V.

12.2 Data Acquisition (DAQ - PCI Express 6259)

National Instruments M Series high-speed multifunction data acquisition (DAQ) devices are optimized for superior accuracy at fast sampling rates. Devices feature fast settling times at high scanning rates, ensuring 16-bit accuracy even when measuring all channels at maximum speeds, noise-reducing, compatible for control applications, 16 analog inputs, 24 digital I/O lines, analog and digital triggering, two counter/timers, contain six DMA channels to maximize data throughput without using PC processing time, with four waveform analog outputs and two 80 MHz counter/timers. M Series devices can execute multiple control loops simultaneously with a single device. For higher-count control loops, with the NI Soft Motion Development Module for LABVIEW and create a complete motion controller with M Series devices. The sampling rate of input is 1.25 MS/s. The sampling rate of output is 2.8 MS/s.

12.3 Data Acquisition (DAQPad-6016)

The National Instruments DAQPad-6016 multifunction data acquisition (DAQ) devices provide plug-and-play connectivity via USB for acquiring, generating, and logging data in a variety of portable and desktop applications. DAQ Pad devices with screw terminals or BNC connectors provide direct connectivity so easily connect sensors and signals without extra cost. Devices feature 16-bit resolution, 16 analog inputs at up to 200 KS/s, 2 analog outputs for accurate output signals and multiple signal connectivity options.

12.4 Function Generation (WAVETEK Model 191)

WAVETEK model 191, a 20 MHz pulse/function generator, is a precision source of sine, triangle, square and pulse waveforms plus DC voltage. All can be externally modulated. Output can be continuous or can be triggered or gated by external signal or front panel switch. Amplitude of the waveforms is variable from 30 V down to 1.5 mV. DC reference of the waveform can be offset positively or negatively.

12.5 Sensor, Actuator and Shaker

QUICKPACK MIDE QP20W double layer piezoelectric type is used as structural sensors, transducers, actuator and shaker attaching them either directly to a data acquisition device. Piezoelectric shall be attached to the main structure by special piezoelectric adhesive. This type of piezoelectric can be used as sensor and actuator at the same time. Piezoelectric and adhesive are shown in figure 11.

13. Experimental System

A smart beam is produced as a test specimen to be used in the experiments for the comparison with simulation results. The smart beam consists of an aluminium beam, piezoelectric patches as an actuator and a sensor. The dimensions and material properties of the smart beam are given in table 3 and table 4. The experimental setup is shown in Figures 12. In the experimental setup, multifunction analog input and analog output (PCI-6259) data acquisition (DAQ) cards of NI are utilized for data acquisition and control action for the sensor and actuator as well as used multifunction analog input and analog output (USB-6016) data acquisition (DAQ) cards is utilized for data acquisition for piezoelectric shaker or used function generation (WAVETEK) to generate harmonic vibration. The sensor voltage (strain rate) data is acquired with the analog input card through the input module. Later, the output signal is simultaneously sent through by the analog output card after a control signal is calculated. Then the control signal is sent to E-507 high voltage amplifier (HVPA) in order to actuate the piezoelectric patch. The input signal to the HVPA is limited by $\pm 2V$ due to the gain of E-507 HVPA is 100. The tip displacements of the beam are measured by calibration between the sensor voltages and tip displacements UZ and hence produced curve fitting equation then program this curve fitting equation in LABVIEW program so that displacement data is available in high accuracy. Personal computers having DAQ cards can work as a controller such a real time control application. Synchronization of multiple DAQ cards is very important for acquiring and sending the data. For the synchronization of DAQ cards used in the closed loop control experiment, time step is 0.001s. The block diagrams of the experimental analysis for free & force vibration are shown in figure 8&9. The codes developed by LABVIEW in this paper are given in Appendix (A1).

14. Closed Loop Simulation of Smart Beam

The finite element model is created using SOLID45 and SOLID5 for the aluminium beam and the PZT patch after material properties are defined to script file in Mechanical APDL ANSYS. Cantilever boundary conditions are applied to the finite element model. The finite element model of the smart beam for free and force vibration

is shown in Figure 13 (a) & (b). The block diagrams of the analysis for free & force vibration are shown in Figure 8 & 9. The active control of a smart beam under free & force forced vibration is analysed. The smart beam is harmonically excited by the piezoelectric shaker at its fundamental frequency. The natural frequencies, uncontrolled and controlled time responses of a cantilever smart beam can be obtain with the simulations. The piezoelectric actuator is placed near the root of the beam to perform effective control. The piezoelectric shaker placed in the middle of the beam to generate evenly harmonic excitation. The different in the result between finite elements and experimental of the time response and frequency domain is related to the FE results are expected to be high since perfect boundary conditions and electromechanical coupling conditions are assumed. However, in the frequency domain, the experimental and simulation results for the first mode are very close to each other as well as in time domain experimental and simulation results are very close to each other.

15. Result and Discussions for Smart Aircraft Wing

The results of free vibration, force vibration and active control vibration are investigated for smart aircraft wing and smart beam. First, the natural frequencies and mode shapes are found with and without piezoelectric patch as well as the effects of changing the position of piezoelectric are presented. Second, the free vibration (displacement response in time domain) for all PZT position is obtained as passive control to select the optimal location for PZT. Third, active control vibration is applied for free and force vibration by used output feedback control to remove the undesired vibration.

15.1 Natural Frequency & Mode Shape

The location of PZT patch on wing is change at three different positions as shown in figure 14 to 16. Natural frequencies and Mode shapes of six natural frequencies for the wing without and with PZT patch at three locations are shown in table 5 and figure 17 to 20. The effect of add piezoelectric as sensor and actuator to the wing is increase the natural frequencies due to the stiffness increase (natural frequency changes directly with stiffness and indirectly with mass) and hence settling time is reduced. This method of changing stiffness of structure is called passive control and will see this effect in the section of free vibration. The effect of changing the location of PZT as sensor and actuator from location 1 to location 2 is decrease the natural frequencies due to the stiffness decrease and hence settling time is increase. The effect of changing the location of piezoelectric as sensor and actuator from location 1 to location 3 is decrease the natural frequencies due to the stiffness decrease and hence settling time is increase. Observe that the stiffness is decrease when the PZT location away from the place of installation.

15.1 Free Vibration due to Aerodynamic Force

The block diagram of the analysis for active vibration control in smart structures is show in figure 8. Maximum aerodynamic force (lift force) is equal to 8176 N at maximum speed of aircraft (316 km/h) for this model [1]. Free vibration response of three cases of aircraft wing is simulated for different control gain (Control OFF & Control ON), time range and actuation voltage. Figures 21 show the tip displacement response of aircraft wing without piezoelectric. The tip displacement responses for sensor and actuator at location 1 are shown in Figures 22 to 26, for location 2 are shown in Figures 27 to 29 and for location 3 are shown in Figures 30 to 32 for the wing with and without active vibration control (Control OFF & Control ON). Observe that from the result of location 1 the best control gain for gain 20 and maximum actuation voltage 500 due to the response reach steady state at 3 sec (smaller settling time and amplitude). While the response reach steady state when control OFF at 15 s. Figure 33 shows the actuation voltage which applied to piezoelectric when controller gain is 20. Figure 34 shows the different between the response for control OFF and control ON of gain 20. Note that from the result of location 2 when comparison with results of location 1 the stiffness and natural frequency are decrease and hence settling time take more time for the response to reach steady state and it is 14 s while for loaction1 settling time is 10s when control OFF as well as the amplitude of location 2 is bigger of amplitude of location 1 as shown in figure 35. However, the best control gain is also for gain 20 and maximum actuation voltage 500 for location 2 due to the smaller settling time and amplitude of tip displacement. Observe that from the result of location 3 when comparison with results of location 1 and 2 the stiffness and natural frequency are decrease and hence settling time take more time for the response to reach steady state and it is 20 s while for loaction1and 2 settling time is 10s and 14s respectively when control OFF as well as the amplitude of location 3 is bigger of amplitude of location 1 as shown in figure 36 and it is the best control gain is also for gain 20 and maximum actuation voltage 500 for location 3. Finally from the results of location 1, 2 and 3 the optimal location for piezoelectric as sensor and actuator is the location 1 due to high stiffness and natural frequency and smaller settling time for passive and active control also in this location maximum strain and stress is produced. Table 6 shows the settling time for all locations with different controller gain and actuation voltage.

15.2 Free Vibration due to Initial Displacement

The block diagram of the analysis for active vibration control in smart structures is shown in figure 9. Initial Displacement 4.4cm is applied to the tip of the wing to obtain the free vibration. The general behaviour of results for this section is similarity to previous section. The tip displacement responses for sensor and actuator at location 1 are shown in Figures 37 to 39, for location 2 are shown in Figures 40 to 42 and for location 3 are shown in Figures 43 to 45 for the wing with and without active vibration control (Control OFF & Control ON). Figure 46 shows the actuation voltage which applied to piezoelectric when controller gain is 20 for location 1. Figure 47 shows the different between the response for control OFF and control ON of gain 20 for location 1. Note that from the result of location 2 & 3 when comparison with results of location 1 the stiffness and natural frequency are decrease and hence settling time take more time for the response to reach steady state ($t_s=15$ for location 2 & $t_s=20$ for location 3) while for location 1 settling time is 10s when control OFF as well as the amplitude of location 2 & 3 is bigger of amplitude of location 1 as shown in figure 48 therefor the best control gain in location 1 is also for gain 20 and maximum actuation voltage 500 due to the smaller settling time and amplitude of tip displacement also in this location maximum strain and stress is produced. Based on the above results the optimal location for piezoelectric as sensor and actuator is the location 1 (near from fixed end) due to high stiffness and natural frequency and smaller settling time for passive and active control. Table 7 shows the settling time for all locations with different controller gain and actuation voltage.

15.3 Force Vibration due to PZT Shaker (Harmonic Excitation)

The block diagram of the analysis for active vibration control in smart structures is shown in figure 10. Harmonic excitation is obtain by piezoelectric shaker and it is produced about ± 4 cm amplitude at the tip of aircraft wing in the form of ($X=X_0 \sin \omega t$) and this amplitude is depend on the voltage which applied to piezoelectric shaker. First mode of the vibration is considered in the feedback (closed loop) control analysis. Force vibration response of smart aircraft wing is simulated for different control gain and different actuation voltage. The piezoelectric is placed at location 1 due to select this location as optimal position for effective piezoelectric as sensor and actuator. The tip displacement response is shown in Figures 49 to 53 for aircraft wing with and without active vibration control. Note that from the results the best control gain is 60 and maximum actuation voltage is 500 due to the amplitude of tip displacement for aircraft wing when control OFF is about ± 4 cm and amplitude when control ON for gain 60 is ± 0.5 mm that mean all undesired vibration are removed and aircraft wing become safe from unwanted vibration which cause crack, fatigue, buckling ...etc. Table 8 shows the amplitude of tip displacement with different controller gain and actuation voltage.

16. Results for Smart Cantilever Beam

The following results for comparison between Mechanical APDL ANSYS and experimental work by using LABVIEW program.

16.1 Natural Frequency & Mode Shape

The location of PZT patch on beam is change at three different positions as shown in figure 54 to 56. Cantilever beam is embedded with three piezoelectric as sensor, actuator and shaker. The location of PZT shaker at the middle of beam and hence natural frequency and stiffness are reduced and settling time is increase in case the sensor and actuator at location 1. The locations of the sensor, actuator and shaker on cantilever beam are shown in figure 57. Natural frequencies and Mode shapes of three natural frequencies are shown in table 9 and figure 58 to 62 for the beam without PZT, with PZT patch at three locations and with PZT shaker. The effect of add piezoelectric as sensor and actuator to the cantilever beam is increase the natural frequencies due to the stiffness increase and hence settling time is reduced. Frequency response is shown in figure 63 (a) & (b).

16.2 Free Vibration

The block diagram of the analysis for active vibration control in smart structures is shown in figure 9. Initial Displacement 1cm is applied to the tip of the cantilever beam to obtain the free vibration. The general behaviour of results and Discussions for smart aircraft wing is similarity to smart beam. Free vibration response of three cases of smart beam is simulated for different control gain, time range and actuation voltage. The piezoelectric sensor and actuator are placed at location 1, 2 & 3. The tip displacement response is shown in Figures (64 a & b) to (65 a & b) for location 1 and for location 2 is shown in Figures (66) to (67) and for location 3 is shown in Figures (68) to (69). Note that from the result of location 2 & 3 when comparison with results of location 1 the stiffness and natural frequency are decrease and hence settling time take more time for the response to reach steady state ($t_s=20$ for location 2 & $t_s=25$ for location 3) while for location 1 settling time is 15s when control OFF as well as the amplitude of location 2 & 3 is bigger of amplitude of location 1 therefor the best control gain in location 1 is gain 12 and maximum actuation voltage 180 due to the smaller settling time and amplitude of tip displacement also in this location maximum strain and stress is produced. Table 10 shows the settling time for all

locations with different controller gain. Figure 70 shows the actuation voltage which applied to piezoelectric when controller gain is 12.

16.3 Force Vibration due to PZT Shaker (Harmonic Excitation)

The block diagram of the analysis for active vibration control in smart structures is shown in figure 9. Harmonic excitation is obtain by piezoelectric shaker and it is produced about ± 4.2 mm amplitude at the tip of smart beam in the form of $(X=X_0 \sin wt)$ and this amplitude is depend on the voltage (200 Volt.) which applied to piezoelectric shaker. First mode of the vibration is considered in the feedback (closed loop) control analysis. Force vibration response of smart beam is simulated for different control gain and different actuation voltage. The piezoelectric is placed at location 1 due to select this location as optimal position for effective piezoelectric as sensor and actuator. The tip displacement response is shown in Figures (71) to (73) for smart beam with and without active vibration control. Observe that from the results the best control gain is 12 due to the amplitude of tip displacement for smart beam when control OFF is about ± 4.2 mm and amplitude when control ON for gain 12 is ± 0.67 mm . Figure 74 shows the different between the response for control OFF and control ON ($K=0$ & $K=12$). Table 11 shows the amplitude of tip displacement with different controller gain for experimental and ANSYS.

17. Conclusions

The main conclusions obtained from the present work are listed below:

1. The location of the piezoelectric as sensor and actuator pair affects the displacement response of the mechanical system. Piezoelectric in location 1 have higher stiffness and natural frequency and smaller settling time as compared with locations 2 & 3 as well as in location 1 maximum strain and stress is produced therefore the optimal location of piezoelectric is location 1.
2. The simulations for the active vibration control of the aircraft wing and beam for free vibration show that the settling time for the vibration reduced effectively and vibration suppression is obtained for various gains, the maximum reduced settling time was from 15 seconds to 3 second.
3. The simulations for the AVC of the aircraft wing and beam for force vibration (Harmonic wave) show that the amplitude for the vibration reduced effectively and vibration suppression is obtained for various gain, the maximum reduced amplitude was from ± 0.04 m to ± 0.0005 m.
4. Output feedback control (AVC) is very effected for vibration reduction when compare it with another type of control such as passive control.
5. The mathematical models are derived by using the finite element method due to complex systems. The computer program APDL ANSYS is used to obtain the mathematical models. Responses of closed loop system are obtained from the block diagrams built in the program by incorporating the control law directly into the finite element programs.
6. Collected control is very important for the stability of mechanical system therefore all the response for aircraft wing and smart beam is stable.
7. The results of the experimental work is matching with result obtain by APDL ANSYS, although there is a little bit amplitude difference between the experimental and simulation amplitudes but the results are good matching.
8. It is observed that the vibration suppression is faster for the increasing actuator size for the same value of the maximum actuator voltage.

References

- [1] Prof. Ugo Galvanetto, Prof. Mirco Zaccariotto and Matteo Scalchi, "Aerodynamic and structural design of some components of an ultra-light aircraft", Anno Academic 2013/2014.
- [2] Weaver W. Jr. and Johnston P.R., "Structural Dynamic by Finite Elements", Prentic-Hall, Englewood Cliffs, N.J., 1987.
- [3] Preumont, A. Vibration control of active structures an introduction (2nd ed.). Netherlands: Kluwer Academic Publishers. 2002
- [4] Allik, H., & Hughes, T.J.R. Finite element method for piezoelectric vibration. International Journal for Numerical Method in Engineering, 2, 151-7.1970
- [5] Sekouri, E. M. Modelling and shape estimation of smart structures for active control, Ph.D Thesis. Quebec University, CANADA.2004.
- [6] ANSYS Structural Analysis Guide, ANSYS Release 15, ANSYS Inc., South Point, Canonsburg, 2004.
- [7] Lin, J. Active control of space structures. C.S. Draper Lab final report R-1454. 1981
- [8] Daniel J. Inman, "Vibration with Control", John Wiley & Sons Ltd, England, 2006.

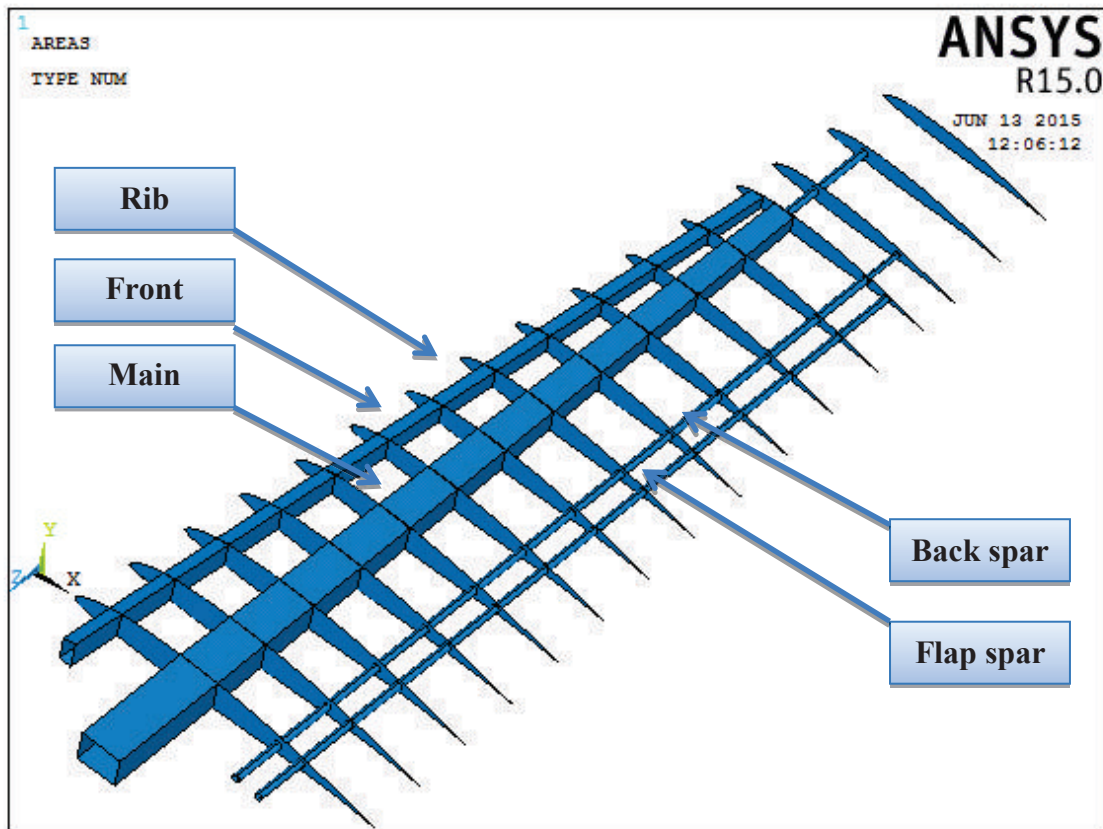


Figure1. Wing Structure

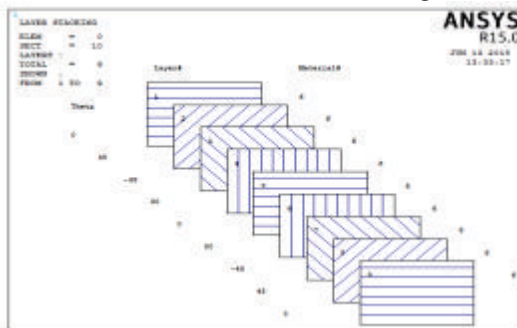


Figure2. Angles of layer

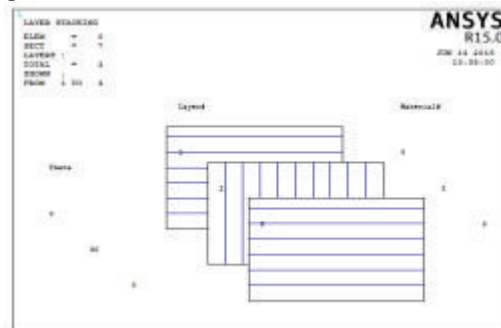


Figure3. Angles of layer

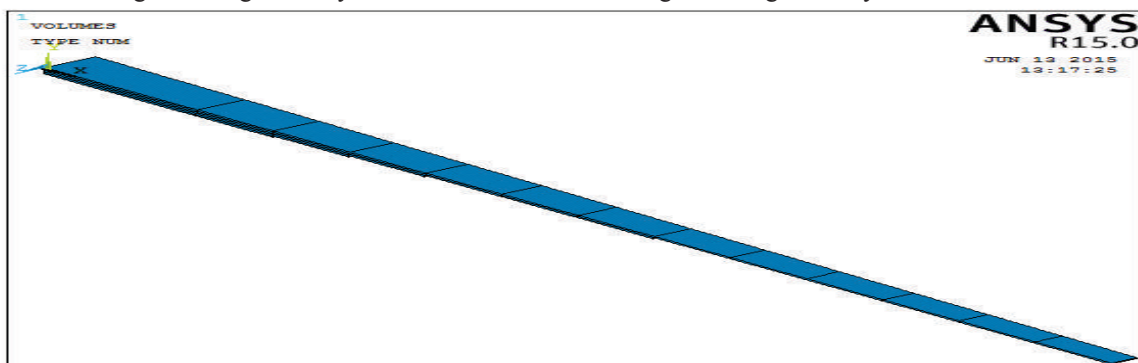


Figure4. Reduction of Thickness on the Main Spar Beams

Table1. Mechanical Properties

Item & Material	Mechanical Properties	
Wing Skin Glass fiber	Density [kg/m ³]	1630
	Modulus of Elasticity E _X [Pa]	15.8E+9
	Modulus of Elasticity E _Y [Pa]	4E+9
	Poisson's ratio ν_{xy}	0.24
	Shear Modulus G _{xy} [Pa]	4.14E+9
Main & Front Spars Silver Fir Wood	Density [kg/m ³]	400
	Modulus of Elasticity E _X [Pa]	10E+9
	Modulus of Elasticity E _Y [Pa]	0.35E+9
	Poisson's ratio ν_{xy}	0.33
	Shear Modulus G _{xy} [Pa]	0.82E+9
Main & Front Spars Birch Plywood	Density [kg/m ³]	720
	Modulus of Elasticity E _X [Pa]	13E+9
	Modulus of Elasticity E _Y [Pa]	0.75E+9
	Poisson's ratio ν_{xy}	0.451
	Shear Modulus G _{xy} [Pa]	1.02E+9
Back, Flap & Front Tip Spars Carbon-Carbon Pipe	Density [kg/m ³]	1600
	Modulus of Elasticity E [Pa]	80E+9
	Poisson's ratio ν_{xy}	0.33
Back Tip Spar Aluminum	Density [kg/m ³]	2780
	Modulus of Elasticity E [Pa]	70E+9
	Poisson's ratio ν_{xy}	0.33
Ribs Flex Foam M-130	Density [kg/m ³]	130
	Modulus of Elasticity E [Pa]	0.108E+9
	Poisson's ratio ν_{xy}	0.49

Table2. Data of Selected Wing

Total Wing span (m)	5
Wing area (m²)	3.208
Aspect ratio	7.79
Taper ratio	0.54166625
Mean aerodynamic chord (m)	0.6643
Root chord (m)	0.8
Tip chord (m)	0.433333
Position of aerodynamic center	X= 0.8148 & Y=0.2566
Sweep angle along leading edge	6.34°
Wing shape	Trapezoidal in X & Y

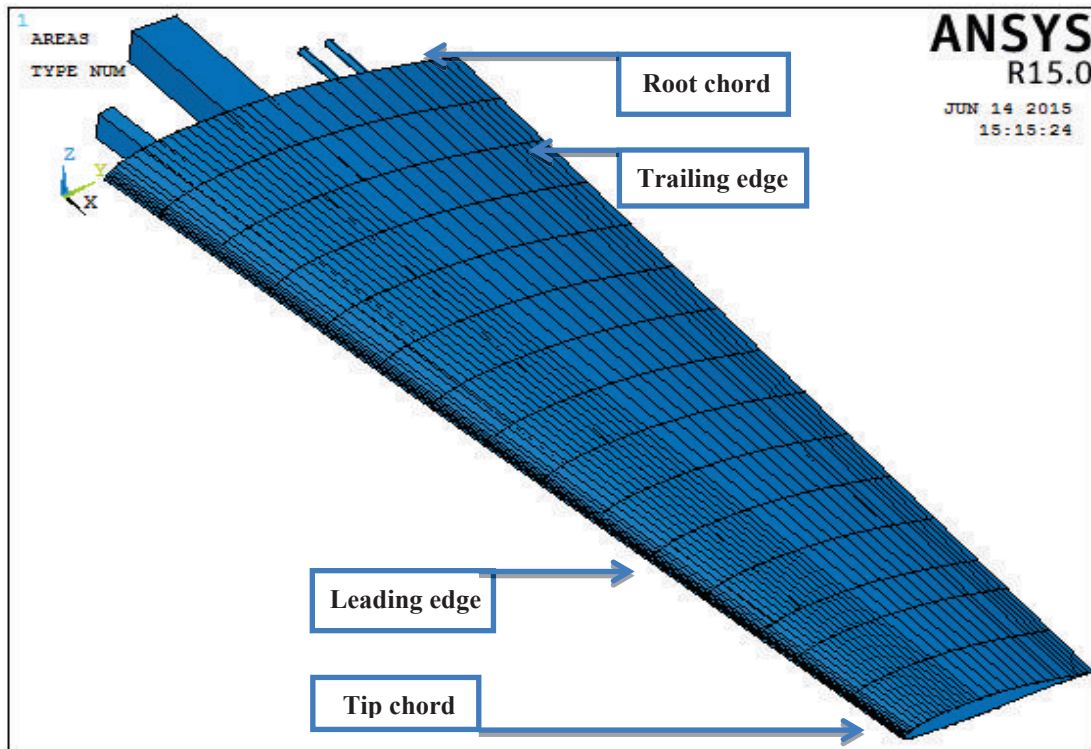


Figure5. Wing Geometry

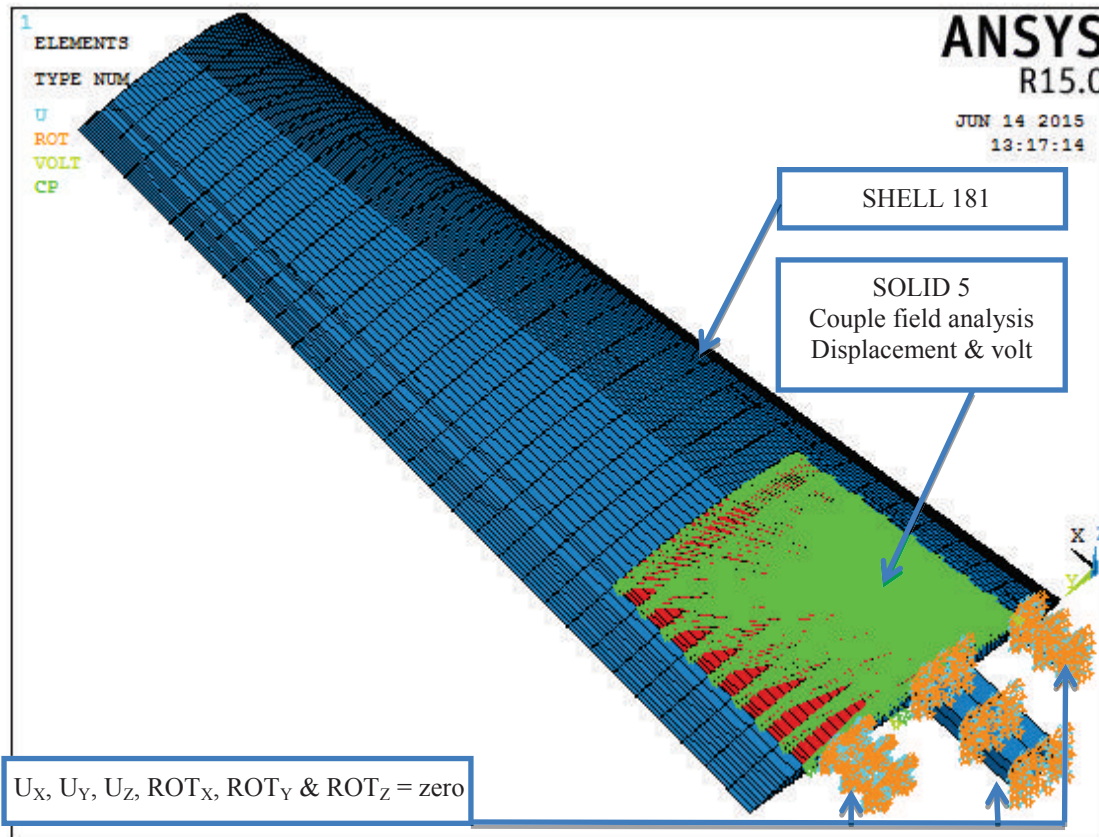


Figure6. Element Type & Boundary Condition

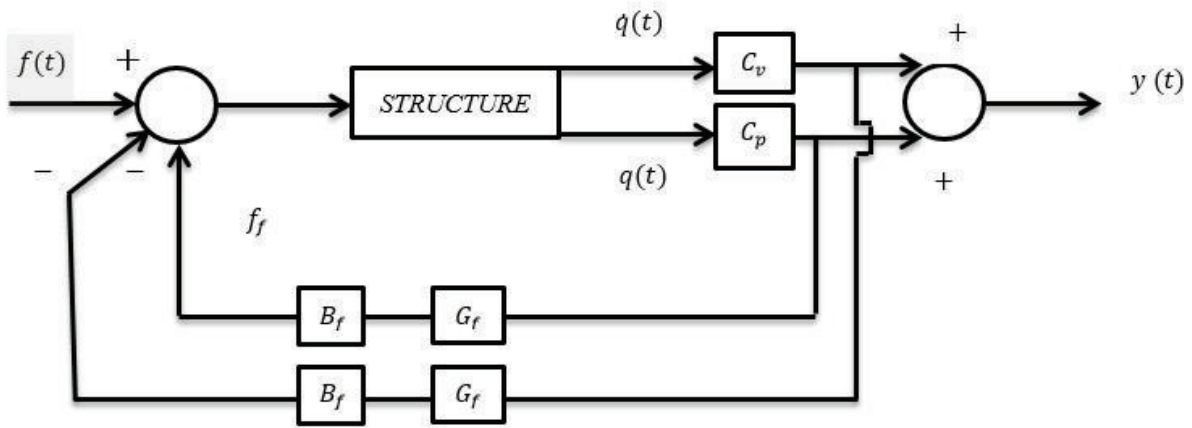


Figure7. Block Diagram of Output Feedback System

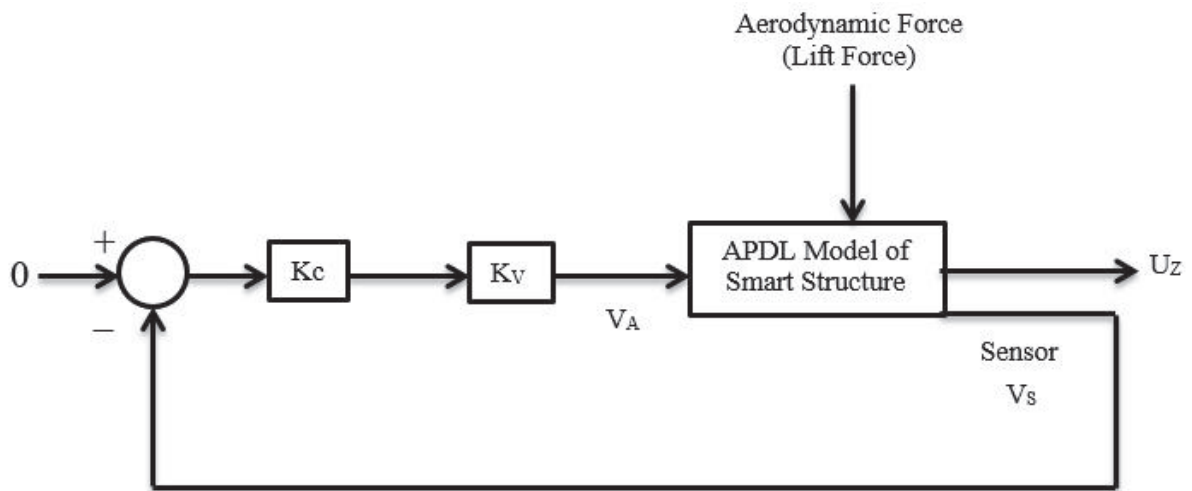


Figure8. Block Diagram of Analysis

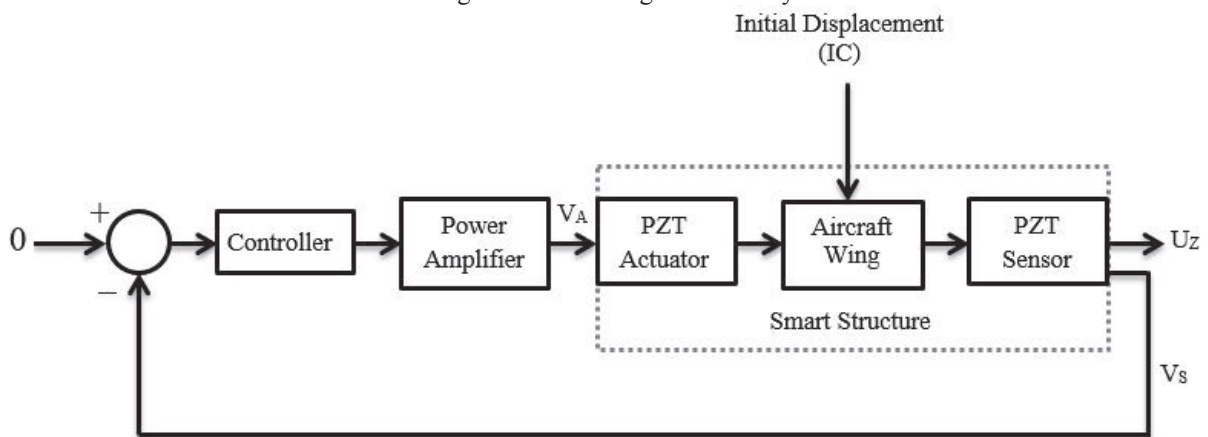


Figure9. Block Diagram of Analysis

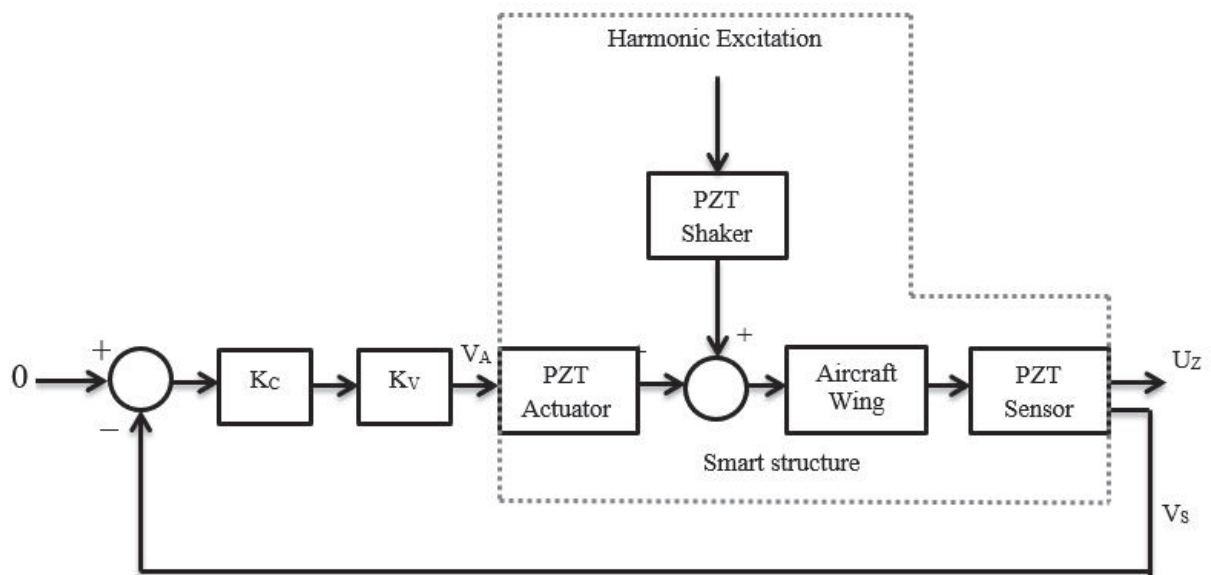


Figure10. Block Diagram of Analysis

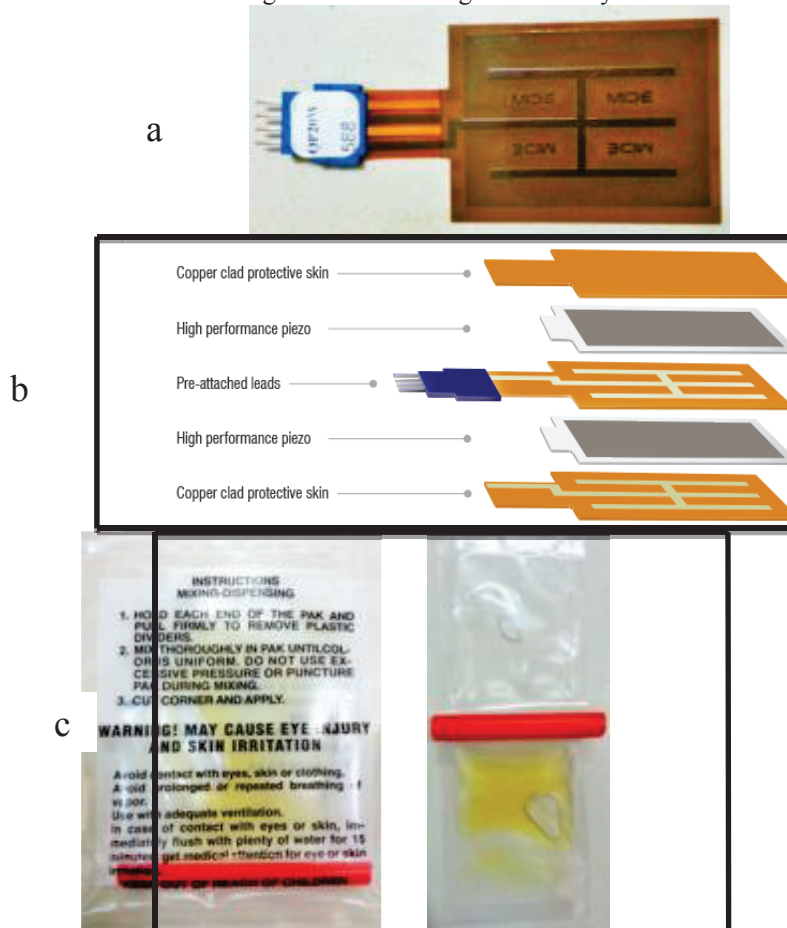


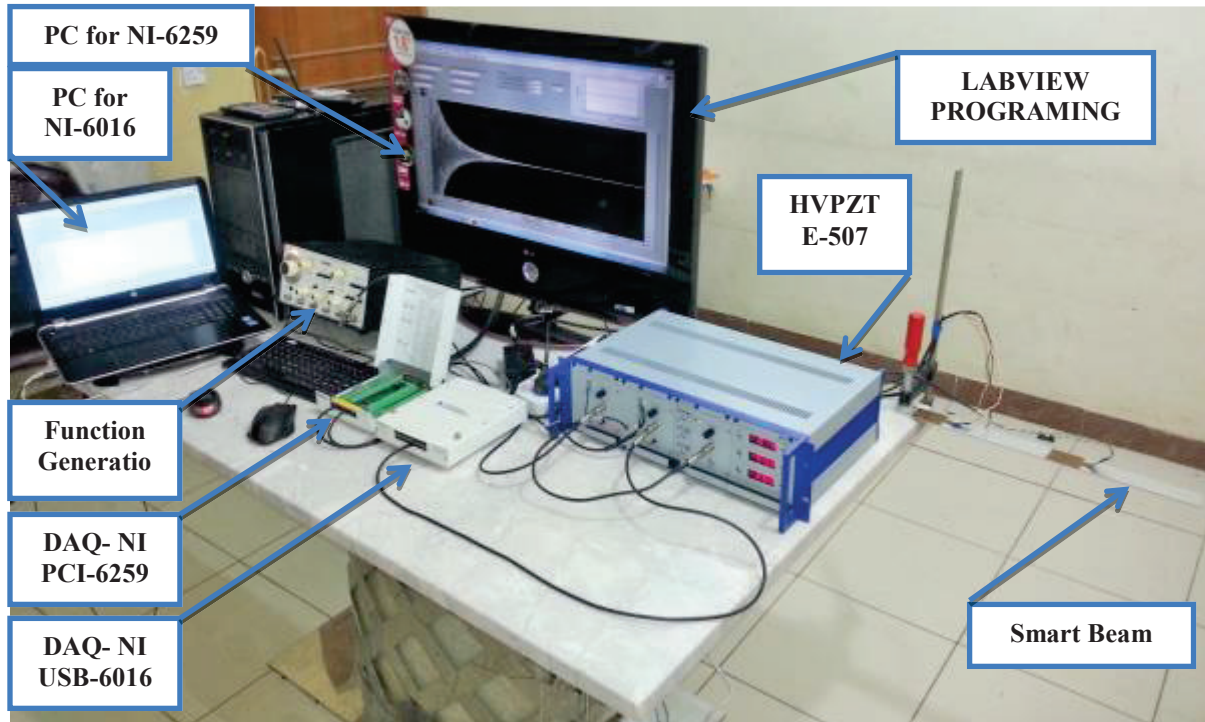
Figure11. (a) Piezoelectric (b) Internal structure of PZT (c) Adhesive

Table3. Dimensions of the Smart Beam

Dimensions	Beam	Piezoelectric
Length	L= 450 mm	LP= 460 mm
Width	B= 40 mm	BP= 33.02 mm
Thickness	H= 1.8 mm	HP= 0.762 mm

Table 4: material properties of the smart beam

Properties	Aluminum
Young modulus	71.7 GPa
Density	2810 kg/m3
Poisson ratio	0.33



Figures12. Experimental Setup

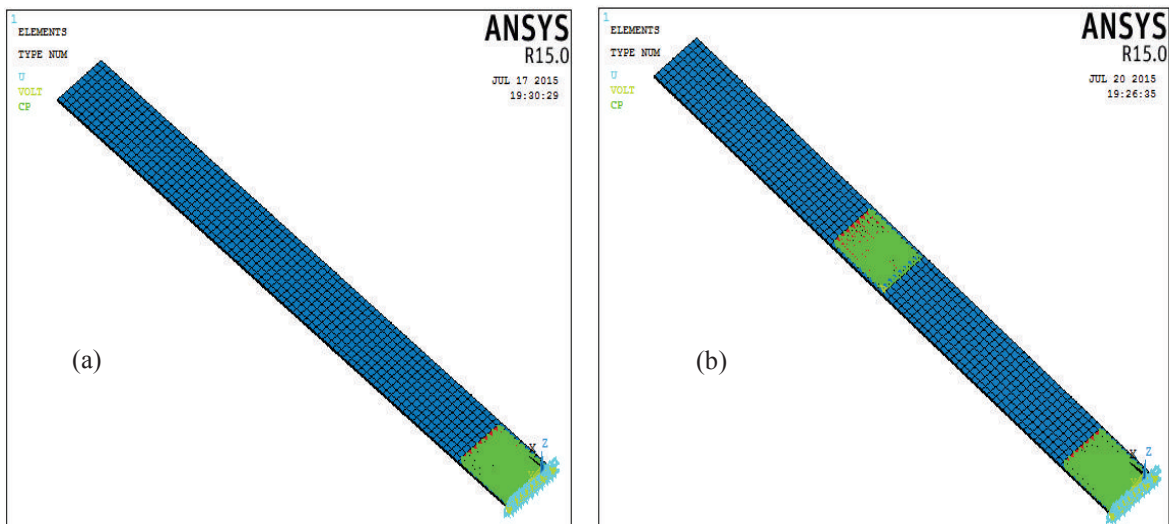


Figure 13 Finite Element Model (a) Free Vibration (b) Force Vibration

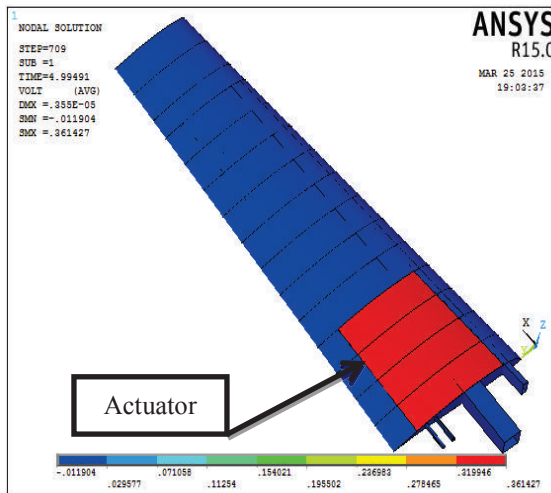


Figure14. (a) Actuator location1

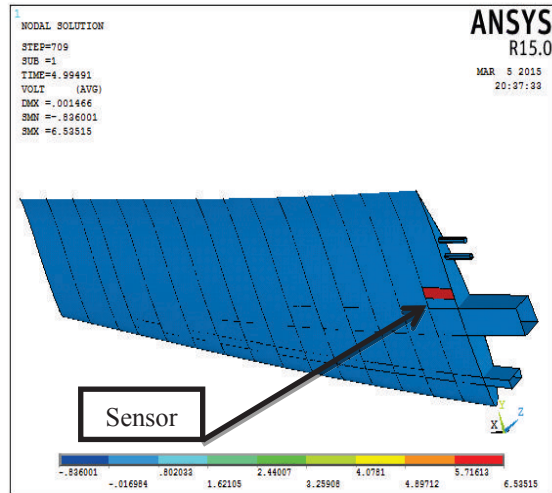


Figure14. (b) Sensor location1

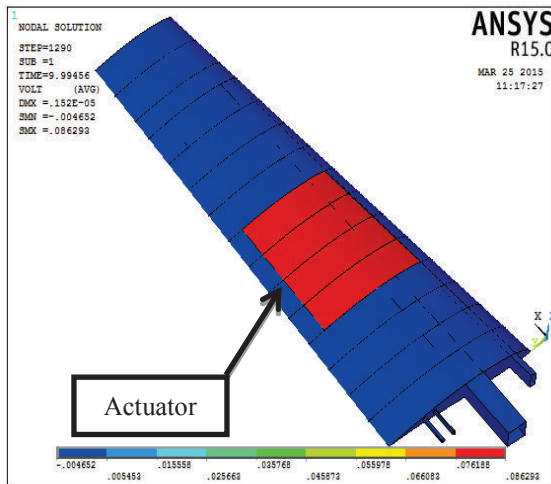


Figure15. (a) Actuator location 2

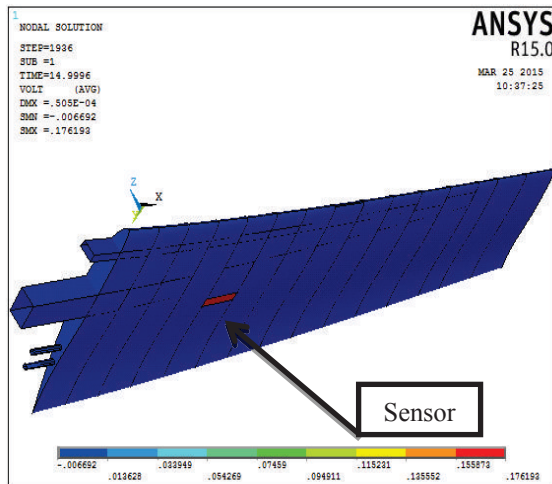


Figure15. (b) Sensor location 2

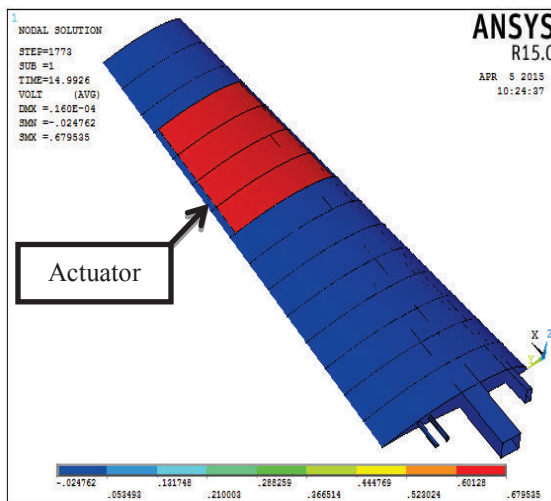


Figure16. (a) Actuator location 3

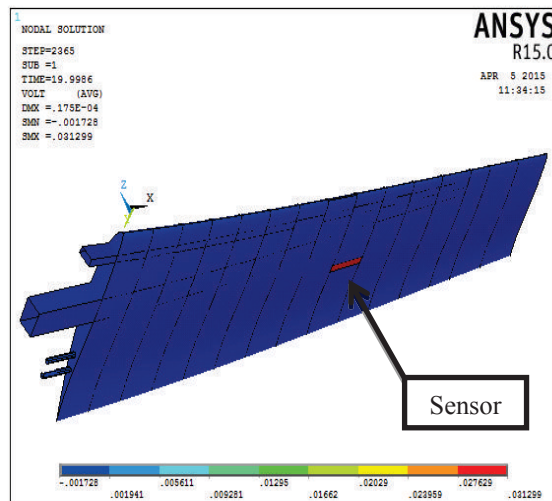


Figure16. (b) Sensor location 3

Table5. Frequency of Aircraft Wing

Frequency HZ	N.F without PZT	N.F with PZT at 1	N.F with PZT at 2	N.F with PZT at 3
f_1	6.2396	7.1695	6.4744	5.9129
f_2	28.701	29.683	28.919	29.967
f_3	36.067	37.182	35.785	34.084
f_4	51.154	53.149	51.278	49.463
f_5	63.859	63.453	64.578	66.307
f_6	98.185	96.062	98.367	99.465

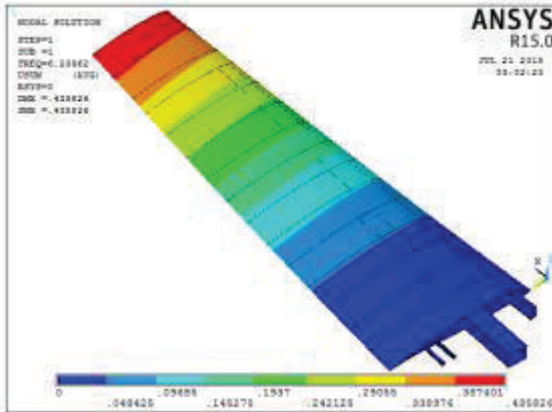


Figure17. (a) First mode shape

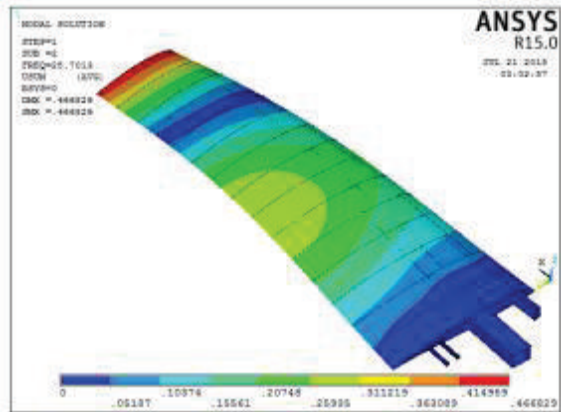


Figure17. (b) Second mode shape

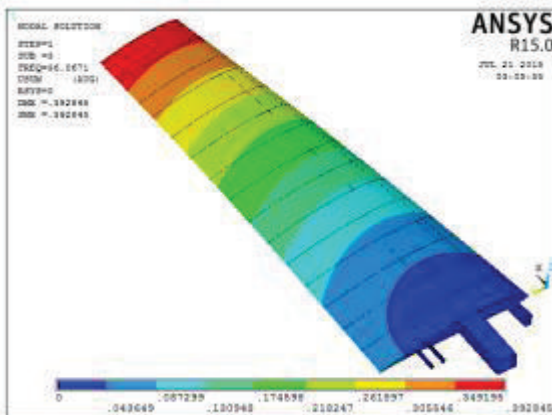


Figure17. (c) Third mode shape

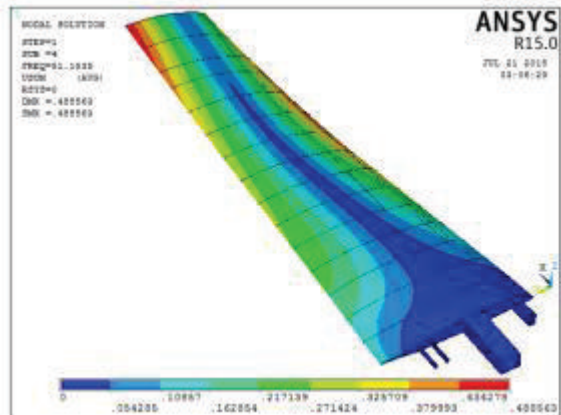


Figure17. (d) Forth mode shape

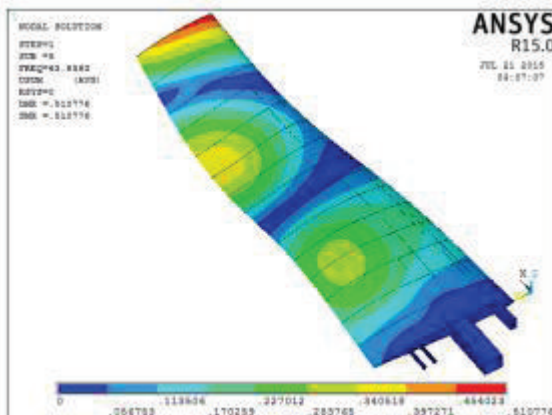


Figure17. (e) Fifth mode shape

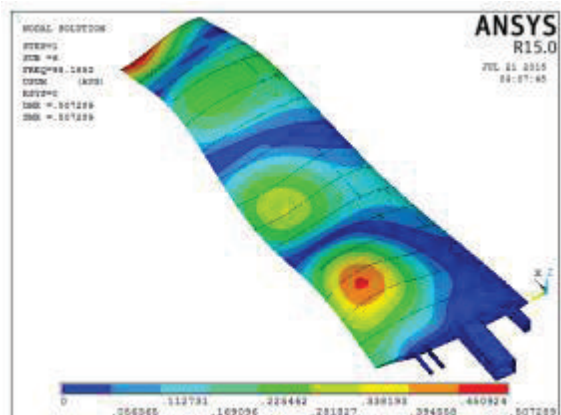


Figure17. (f) Sixth mode shape

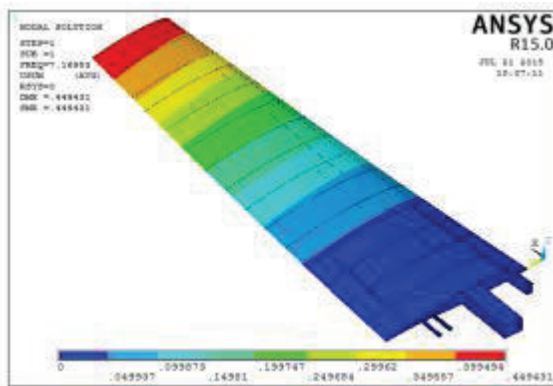


Figure18. (a) First mode shape at PZT1

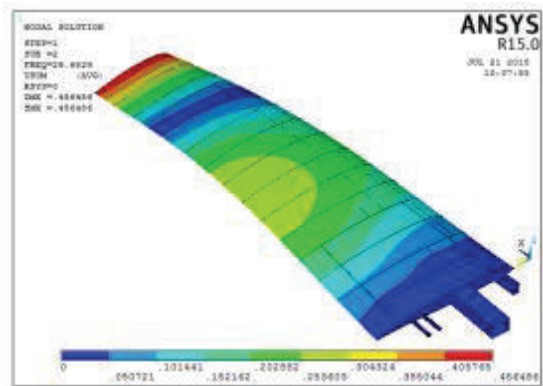


Figure18. (b) Second mode shape at PZT1

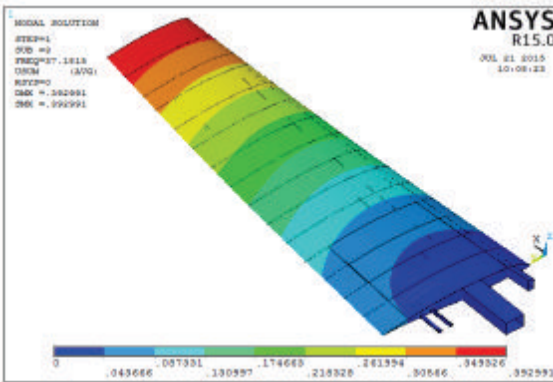


Figure18. (c) Third mode shape at PZT1

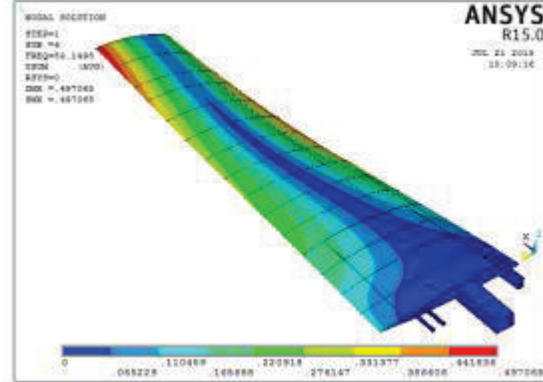


Figure18. (d) Forth mode shape at PZT1

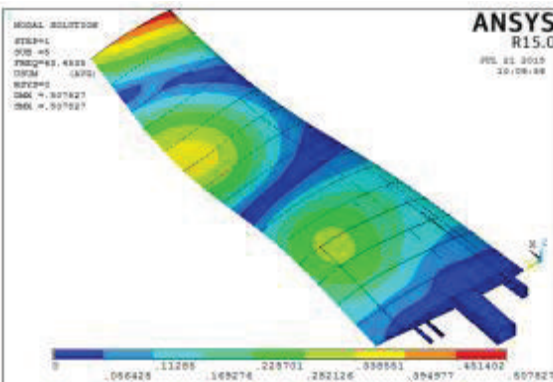


Figure18. (e) Fifth mode shape at PZT1

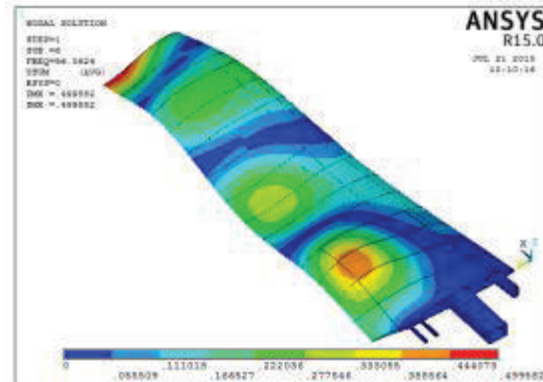


Figure18. (f) Sixth mode shape at PZT1

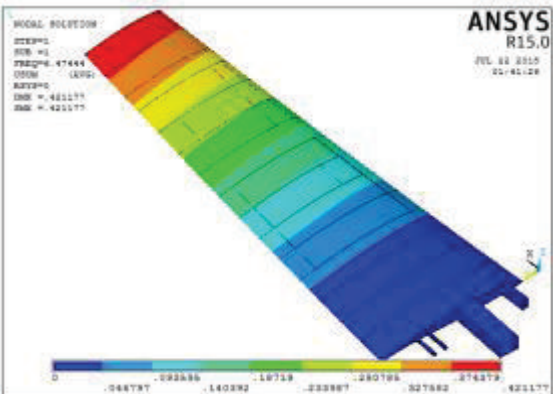


Figure19. (a) First mode shape at PZT2

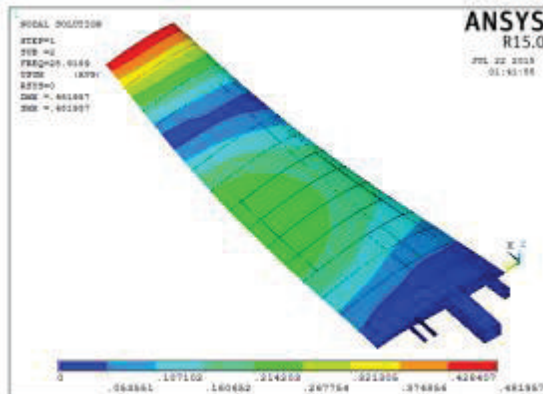


Figure19. (b) Second mode shape at PZT2

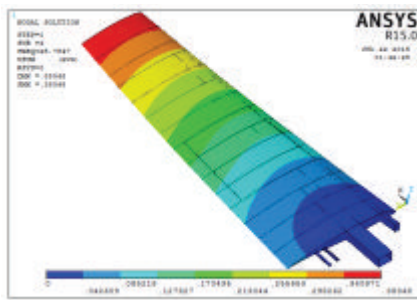


Figure19. (c) Third mode shape at PZT2

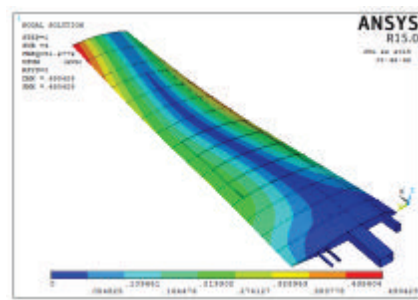


Figure19. (d) Forth mode shape at PZT2

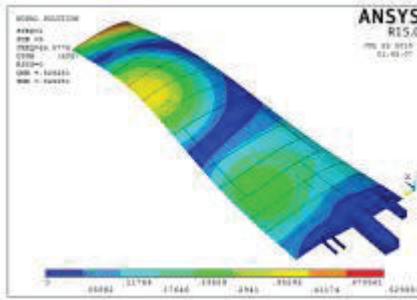


Figure19. (e) Fifth mode shape at PZT2

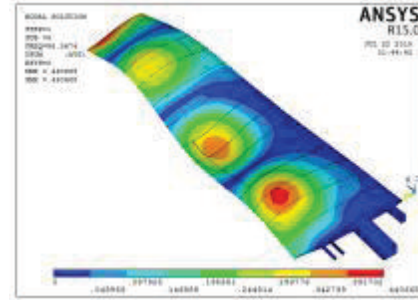


Figure19. (f) Sixth mode shape at PZT2

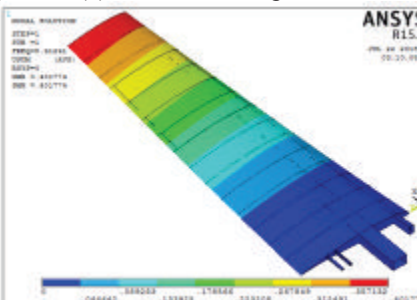


Figure20. (a) First mode shape at PZT3

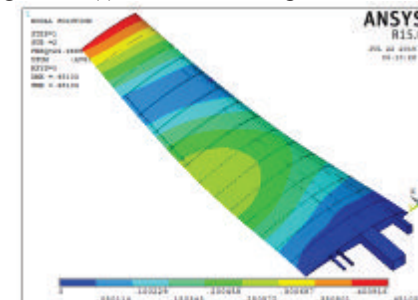


Figure20. (b) Second mode shape at PZT3

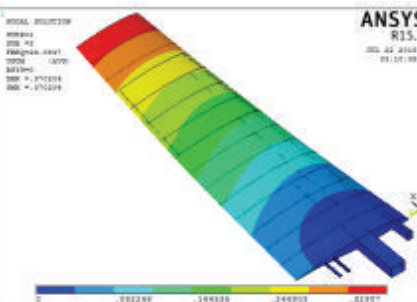


Figure20. (c) Third mode shape at PZT3

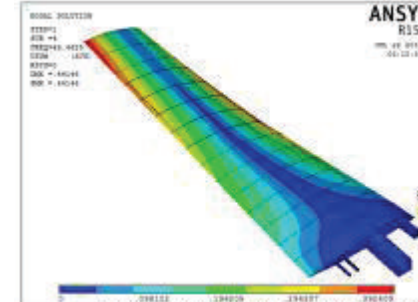


Figure20. (d) Forth mode shape at PZT3

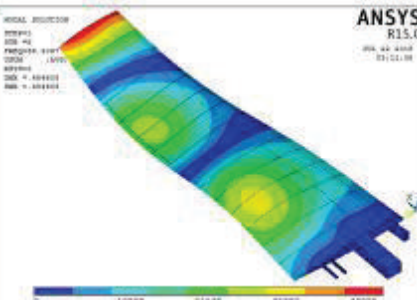


Figure20. (e) Fifth mode shape at PZT3

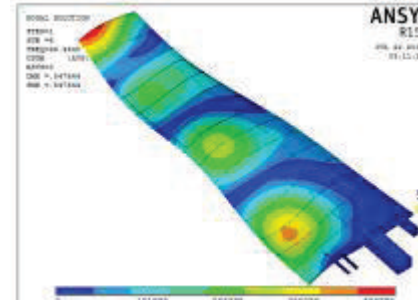


Figure20. (f) Sixth mode shape at PZT3

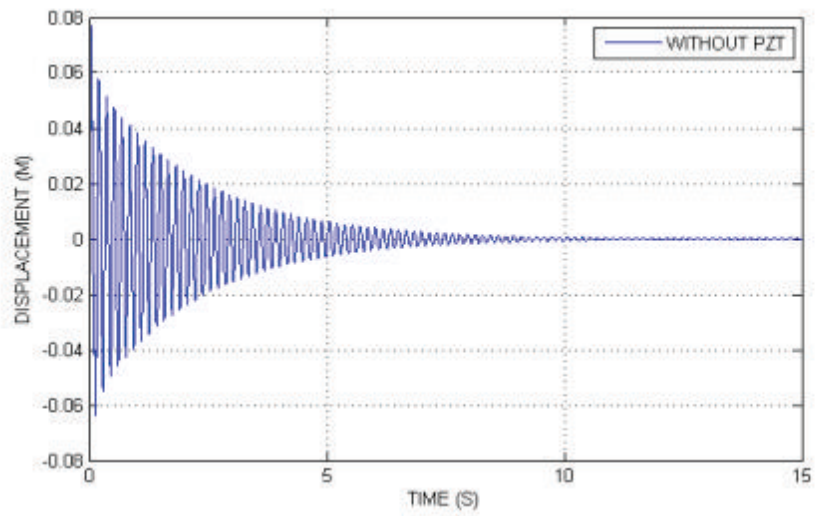


Figure 21. Tip Displacements Response

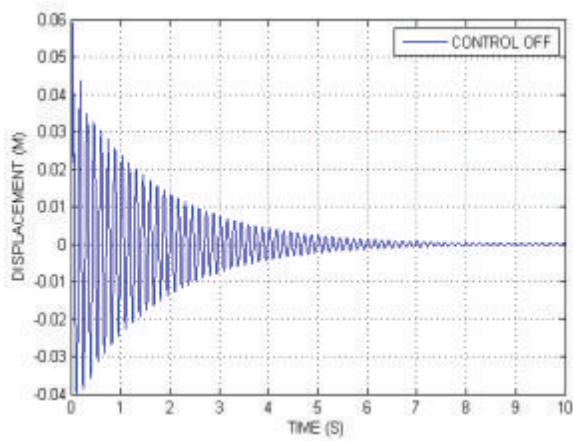


Figure 22. (a) Tip displacement Response (K=0)

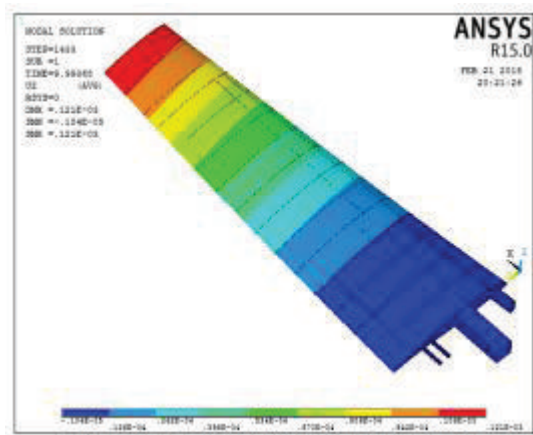


Figure 22. (b) Displacement at time step 10s

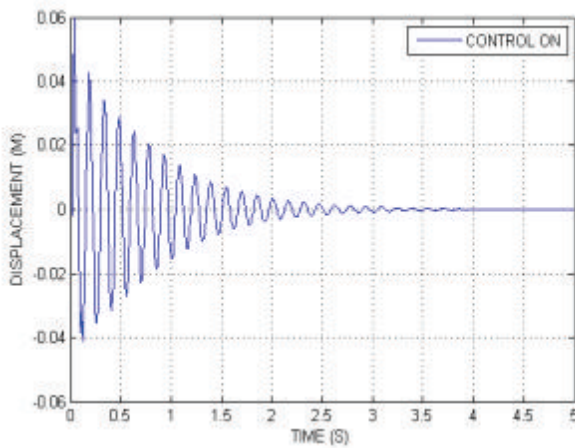


Figure 23. (a) Tip displacement Response (K=10, V max. =500)

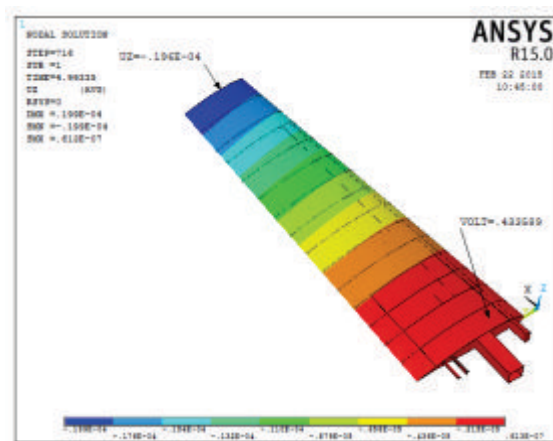


Figure 23. (b) Displacement at time step 5s

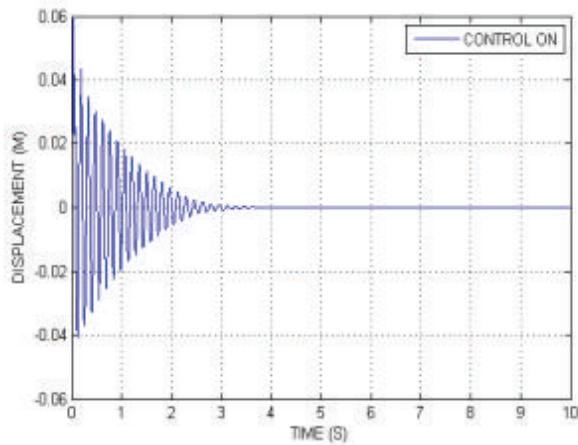


Figure24. (a) Tip displacement Response (K=20, V max. =270)

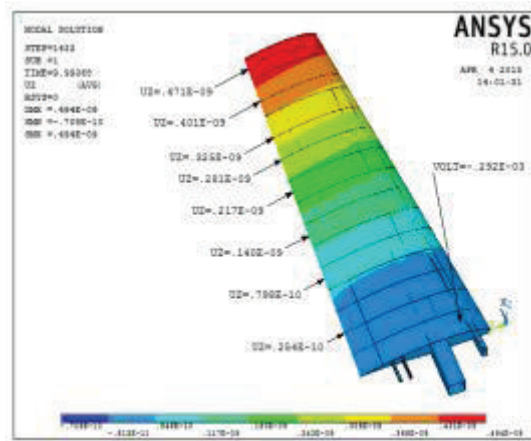


Figure24. (b) Displacement at time step 10s

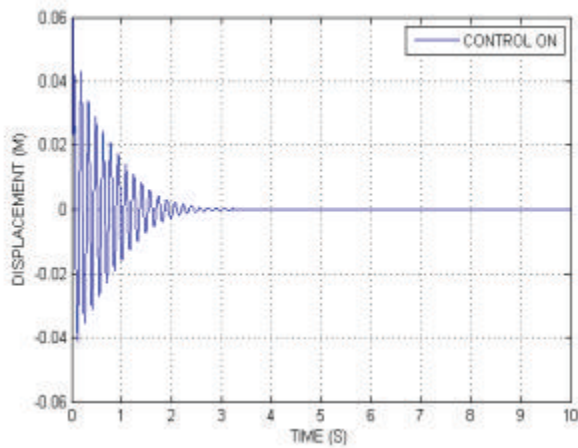


Figure25. (a) Tip displacement Response (K=20, V max. =500)

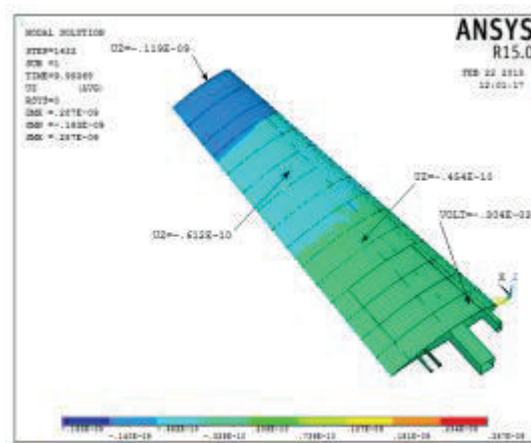


Figure25. (b) Displacement at time step 10s

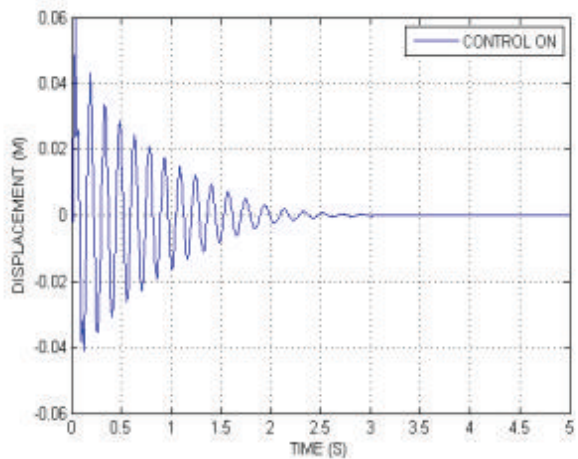


Figure26. (a) Tip displacement Response (K=40, V max. =500)

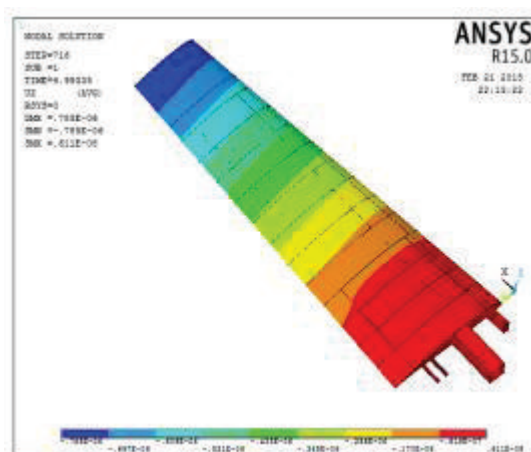


Figure26. (b) Displacement at time step 5s

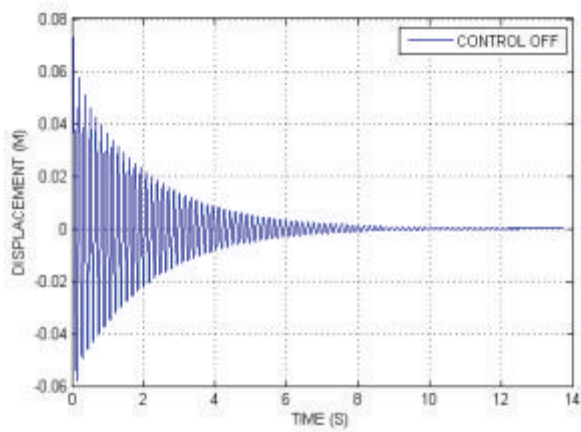


Figure27. Tip displacement Response (K=0)

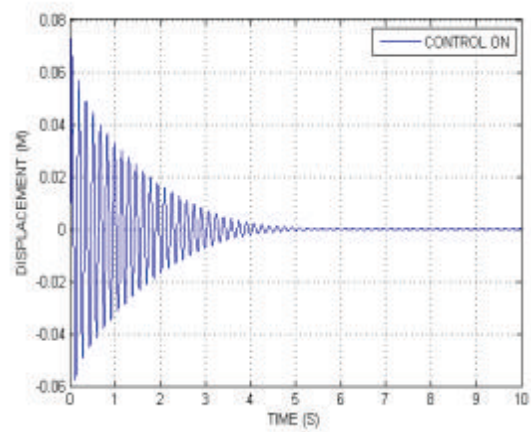


Figure28. Tip displacement Response (K=20, V max. =270)

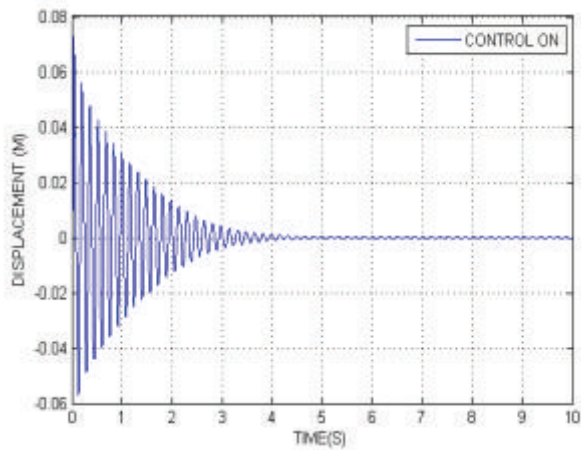


Figure29. Tip displacement Response (K=20, V max. =500)

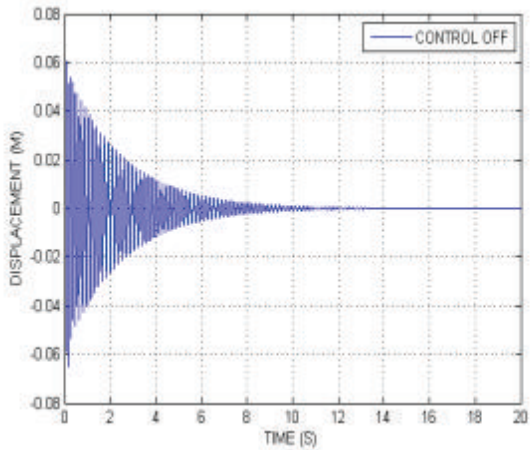


Figure30. Tip displacement Response (K=0)

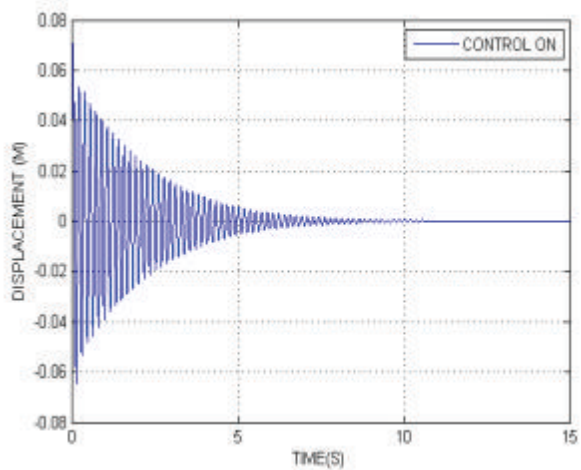


Figure31. Tip displacement Response (K=20, V max. =270)

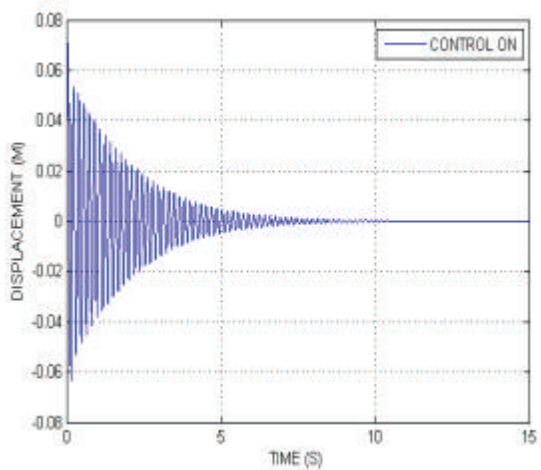


Figure32. Tip displacement Response (K=20, V max. =500)

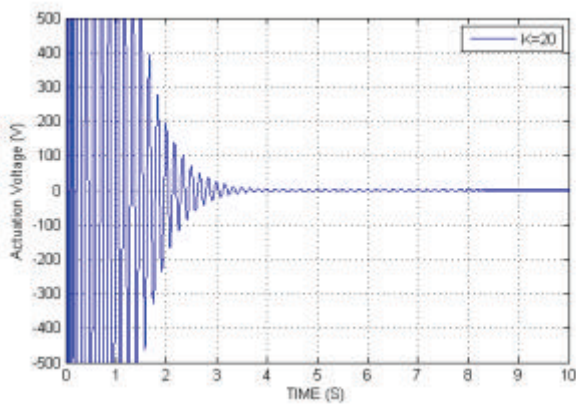


Figure33. Actuation Voltage for K=20

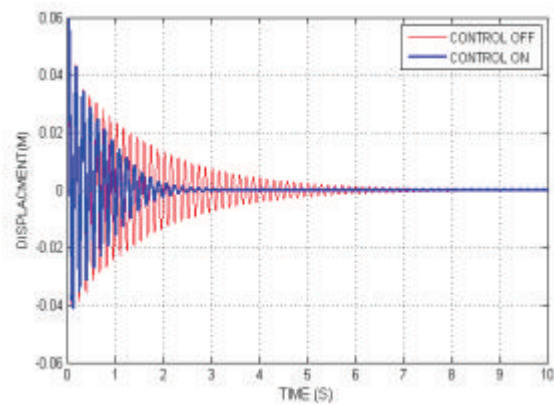


Figure34. Different between response K=20

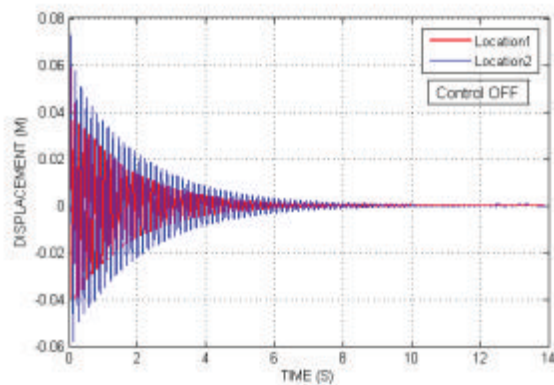


Figure35. Different between the Responses

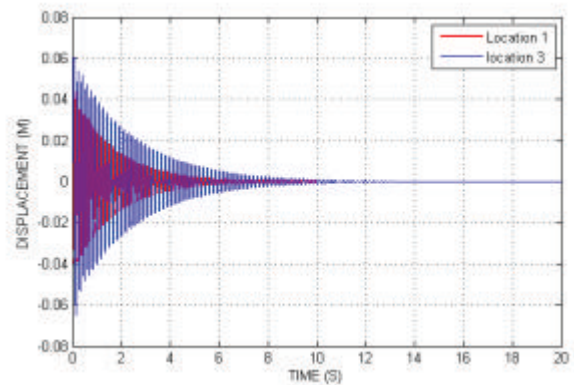


Figure36. Different between the Responses

Table6. Settling Time

Control Gain (K)	Max. Actuation Voltage	Settling Time(s)		
		Location 1	Location 2	Location 3
0	0	10	14	20
20	270	4	7	13
20	500	3	5	10

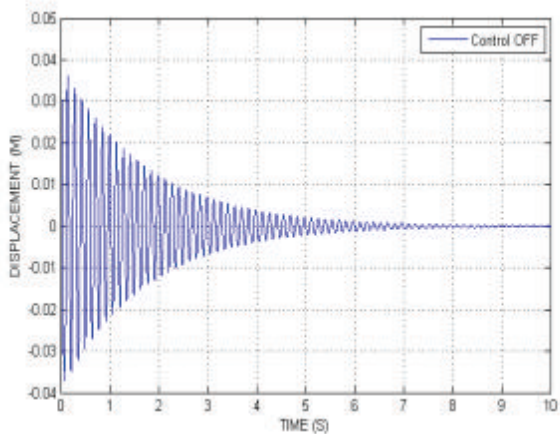


Figure37. Tip displacement Response (K=0)

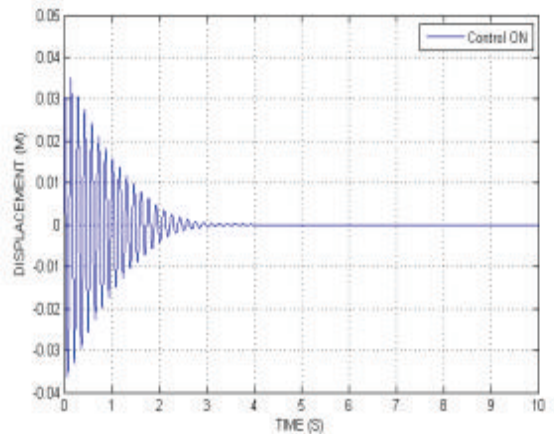


Figure38. Tip displacement Response (K=20, V max. =270)

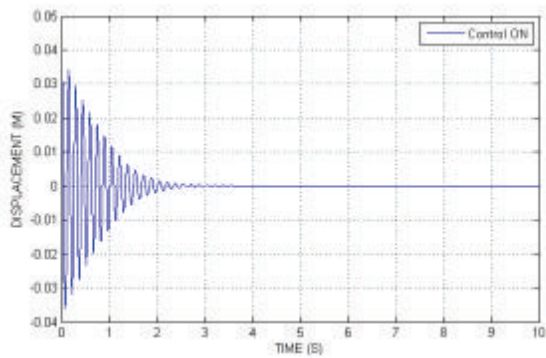


Figure39. Tip displacement Response (K=20, V max. =500)

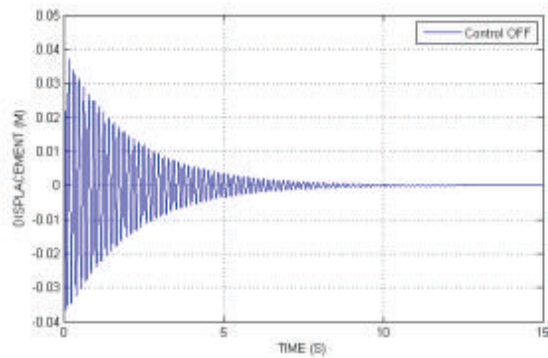


Figure 40. Tip displacement Response (K=0)

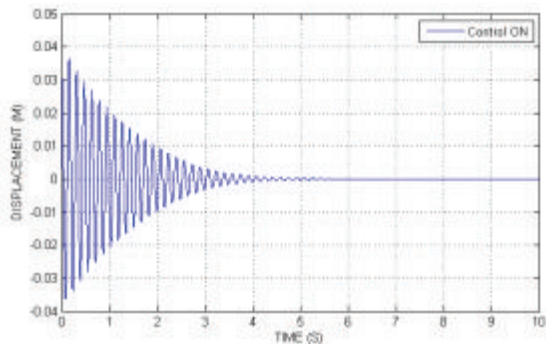


Figure41. Tip displacement Response (K=20, V max. =270)

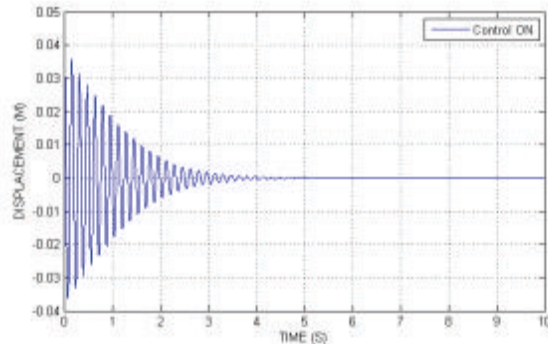


Figure42. Tip displacement Response (K=20, V max. =500)

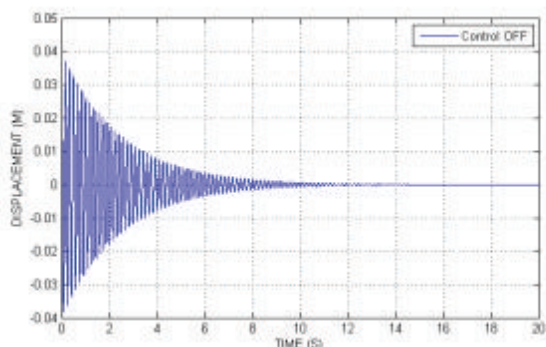


Figure 43 Tip displacement Response (K=0)

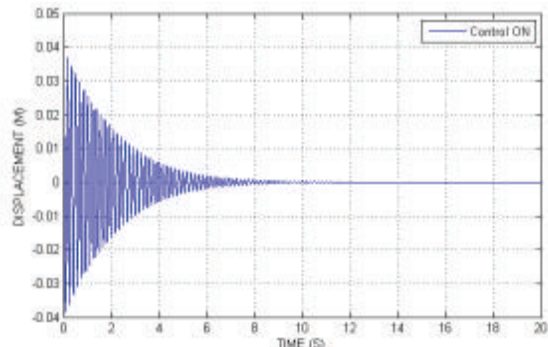


Figure 44 Tip displacement Response (K=20, V max. =270)

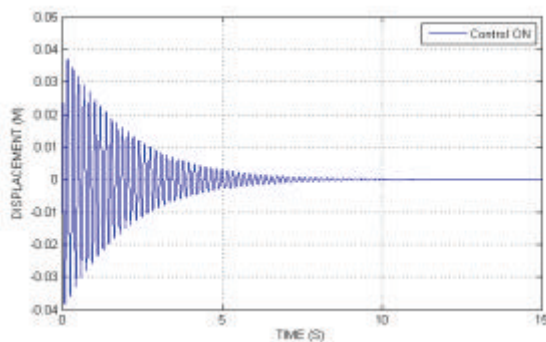


Figure 45 Tip displacement Response (K=20, V max. =500)

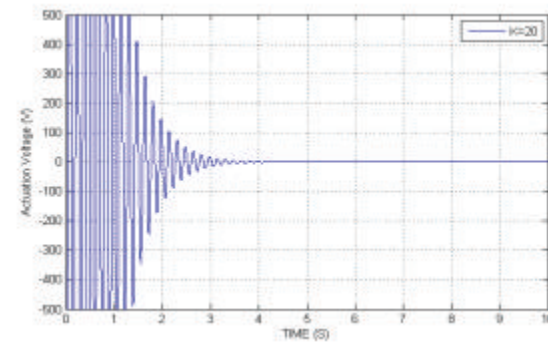


Figure46. Actuation Voltage for K=20

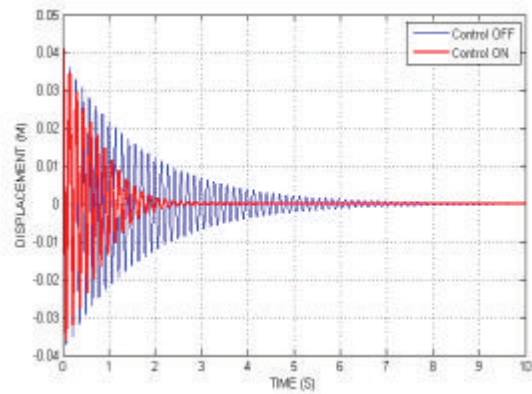


Figure47. Different between response K=20

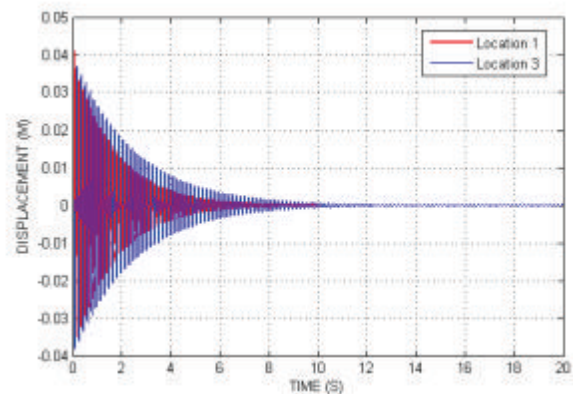


Figure48. Different between the responses

Table7. Settling Time

Control Gain (K)	Max. Actuation Voltage	Settling Time(s)		
		Location 1	Location 2	Location 3
0	0	10	15	20
20	270	4	5.5	11
20	500	3	4.8	10.2

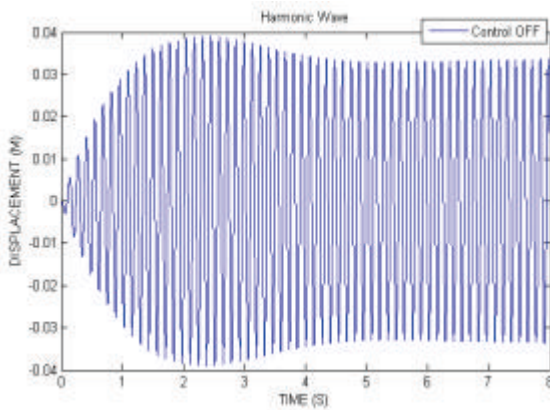


Figure49. Tip displacement Response (K=0)

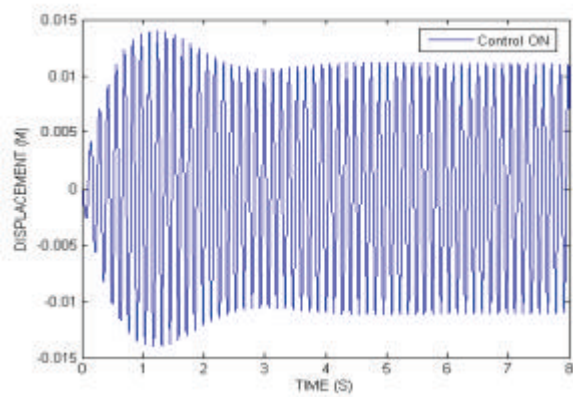


Figure50. Tip displacement Response (K=20, V max. =270)

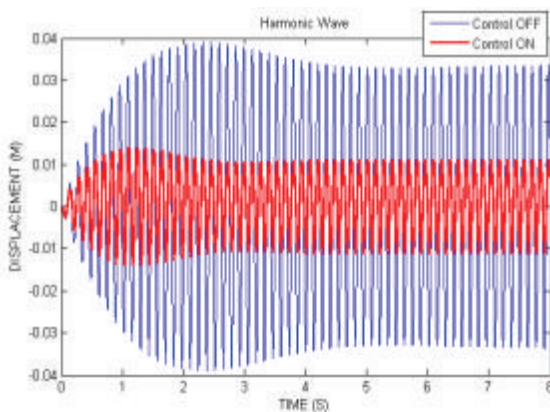


Figure51. Different between responses for K=0 and K=20 (V Max. =270)

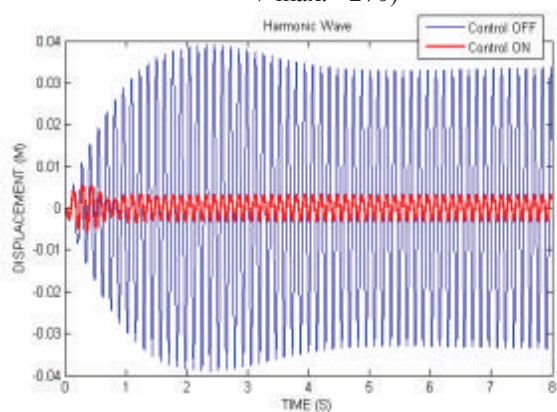


Figure52. Different between responses for K=0 and K=20 (V Max. =500)

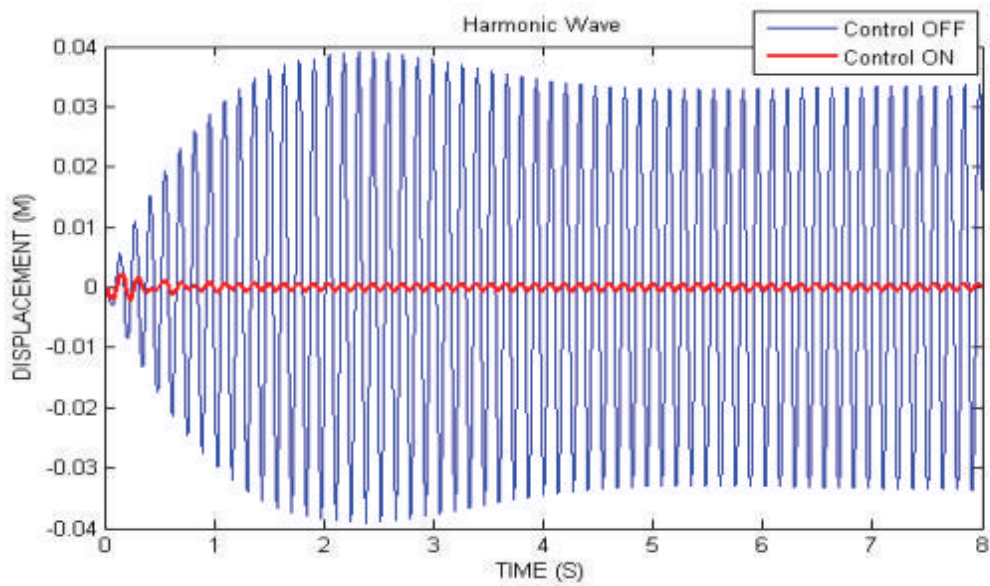


Figure53. Different between response for K=0 and K=60 (V Max. =500)

Table8. Amplitude of Tip Displacement

Control Gain (K)	Max. Actuation Voltage	Amplitude (M)
0	0	± 0.04
20	270	± 0.011
20	500	± 0.0031
60	500	± 0.0005

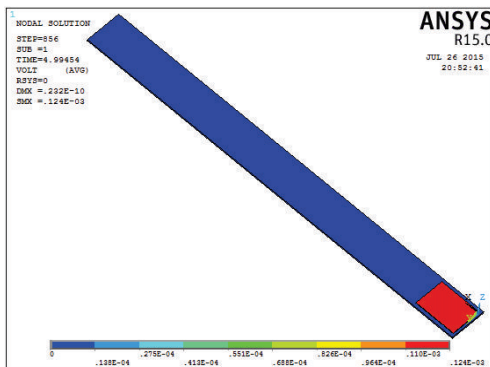


Figure54. PZT locations 1

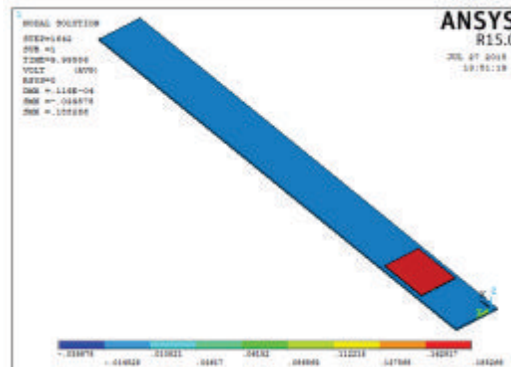


Figure55. PZT locations 2

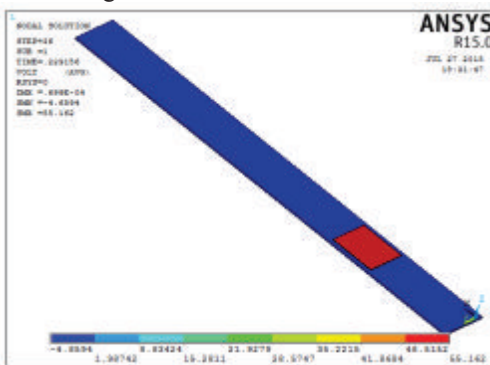


Figure56. PZT locations 3

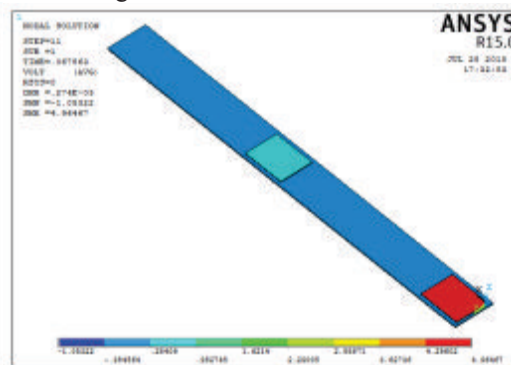


Figure57. PZT Shaker location

Table9. Natural frequencies

Frequency HZ	Without PZT	Experimental	ANSYS			With PZT Shaker	
		Location 1	Location 1	Location 2	Location 3	Experimental	ANSYS
f_1	7.3170	8.2	8.5938	8.2249	7.8615	7.59	8.1046
f_2	45.853	51	52.676	45.784	43.301	51	50.435
f_3	128.55	142	144.09	121.41	121.96	138	138.30

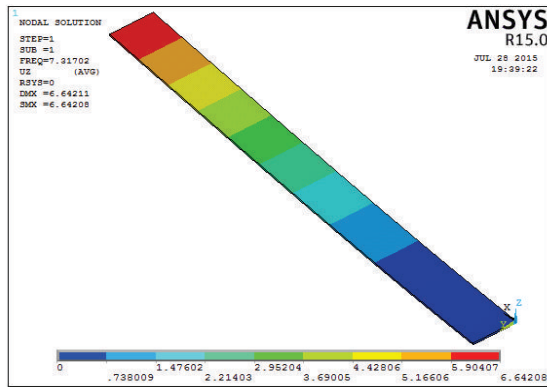


Figure58. (a) First mode shape

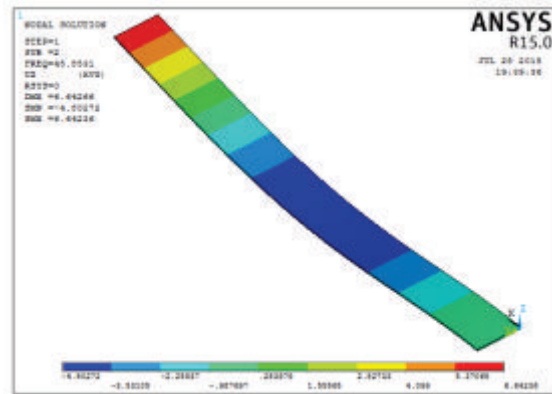


Figure58. (b) Second mode shape

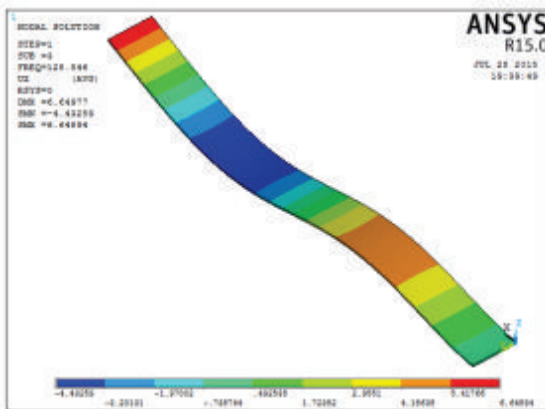


Figure58. (c) Third mode shape

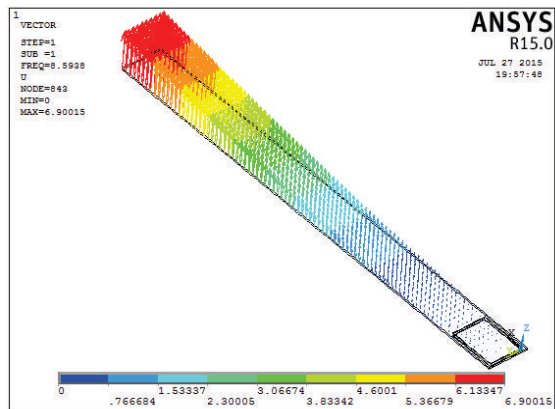


Figure59. (a) First mode shape at PZT1

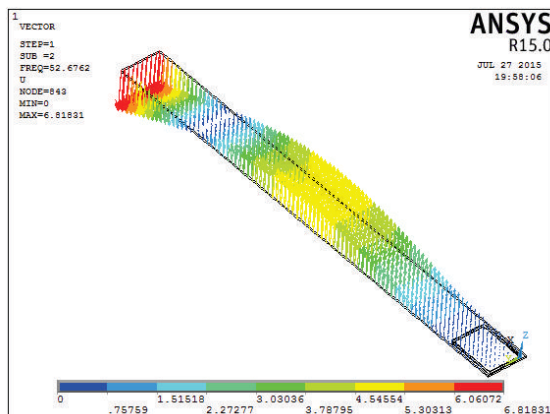


Figure59. (b) Second mode shape at PZT1

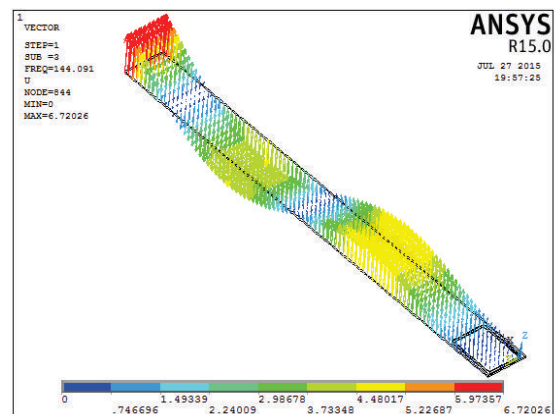


Figure59. (c) Third mode shape at PZT1

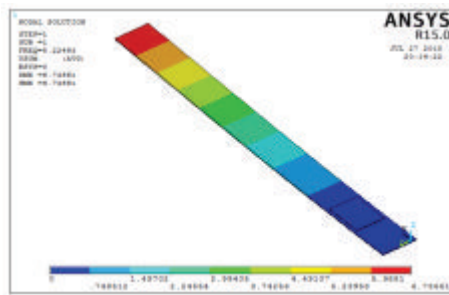


Figure60. (a) First mode shape at PZT2

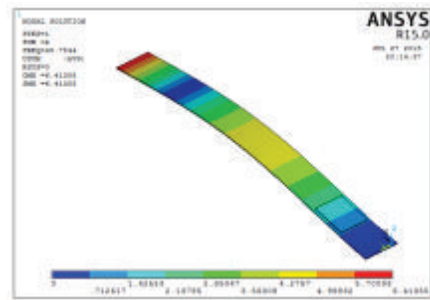


Figure60. (b) Second mode shape at PZT2

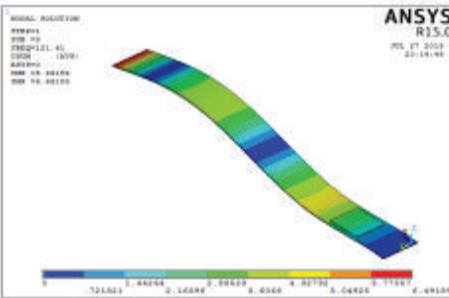


Figure60. (c) Third mode shape at PZT2

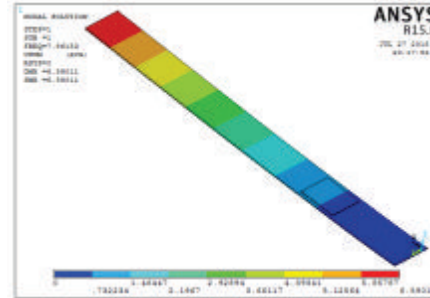


Figure61. (a) First mode shape at PZT3

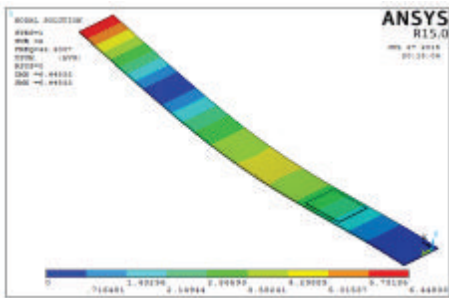


Figure61. (b) Second mode shape at PZT3

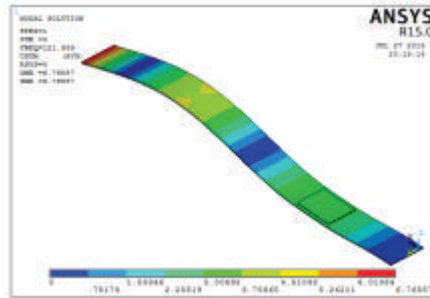


Figure61. (c) Third mode shape at PZT3

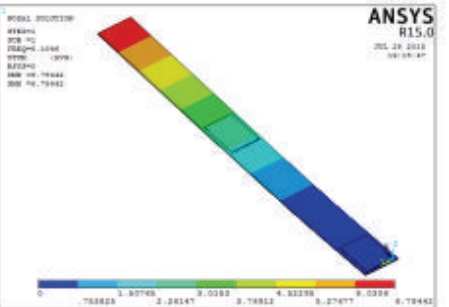


Figure62. (a) First mode shape with Shaker

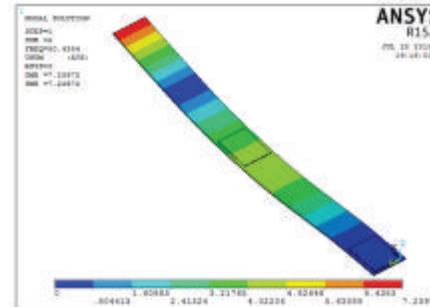


Figure62. (b) Second mode shape with Shaker

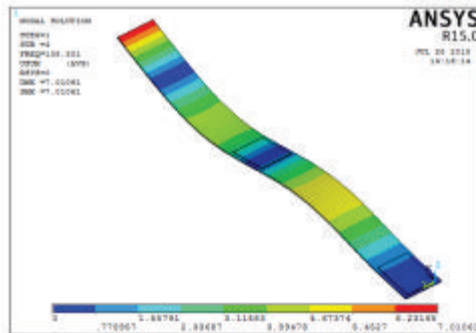


Figure62. (c) Third mode shape with Shaker

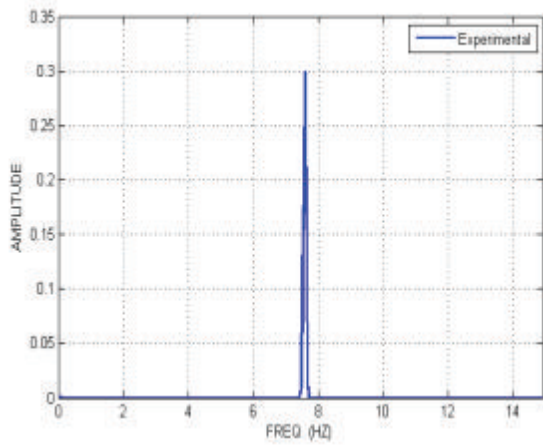


Figure63. (a) Experimental Frequency Response with Shaker

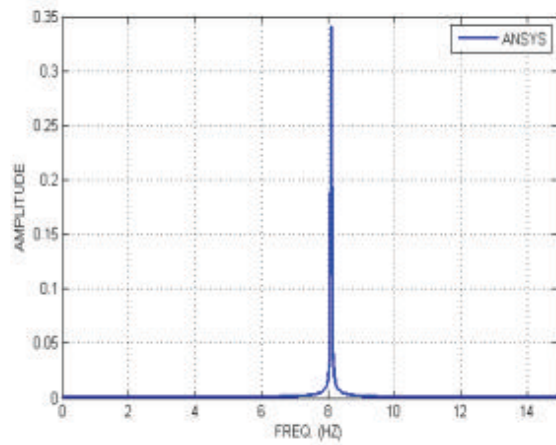


Figure 63. (b) ANSYS Frequency Response with Shaker

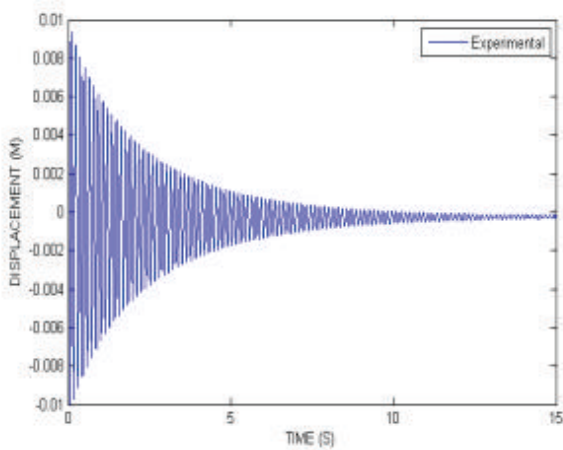


Figure64. (a) Experimental Tip displacement Response (K=0)

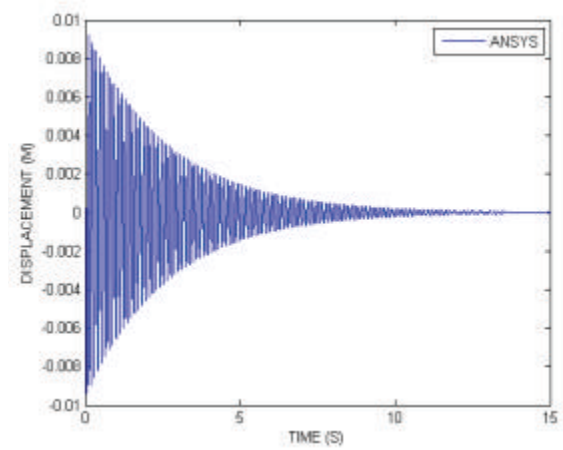


Figure64. (b) ANSYS Tip displacement Response (K=0)

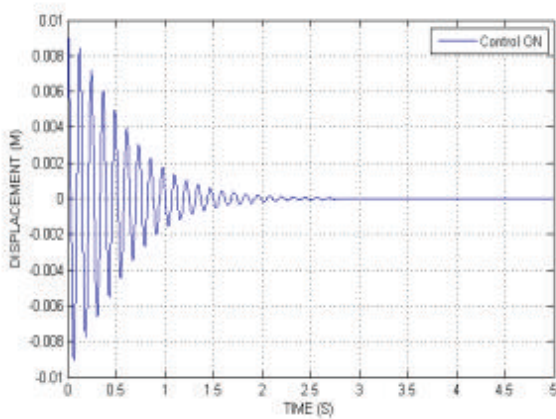


Figure65. (a) Experimental Tip displacement Response (K=12)

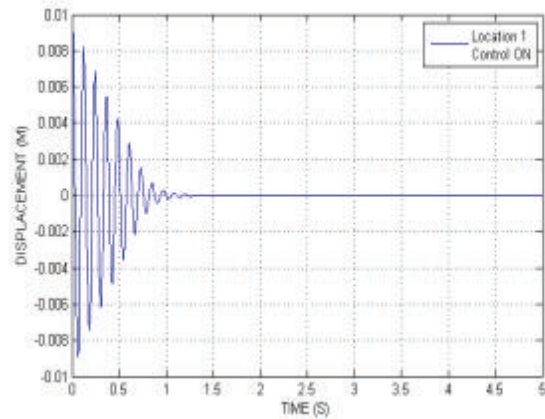


Figure65. (b) ANSYS Tip displacement Response (K=12)

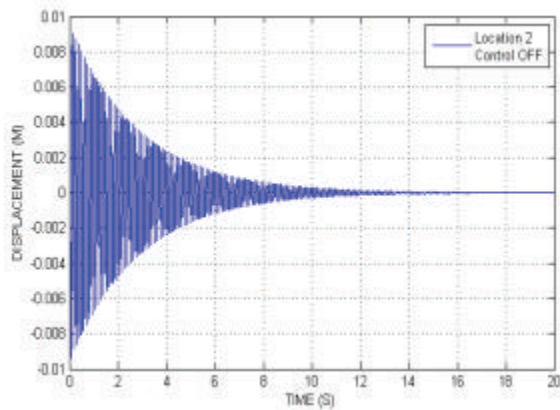


Figure66. Tip displacement Response (K=0)

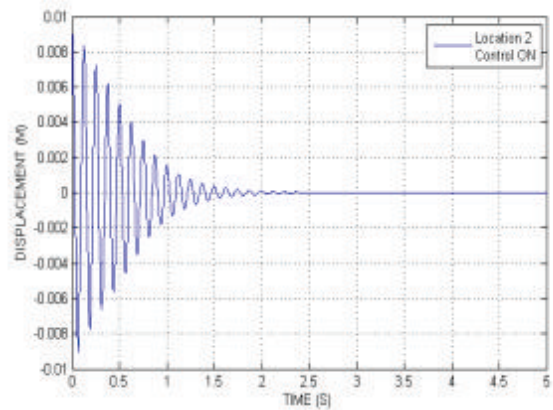


Figure67. Tip displacement Response (K=10)

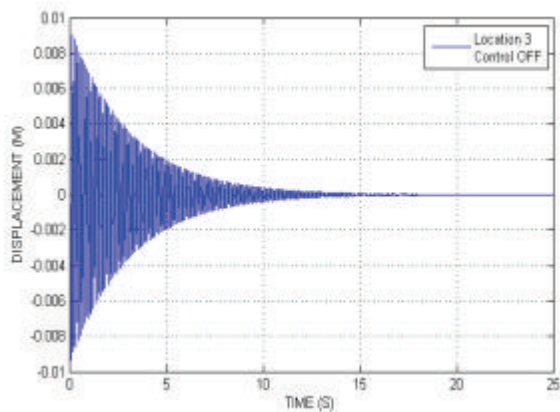


Figure68. Tip displacement Response (K=0)

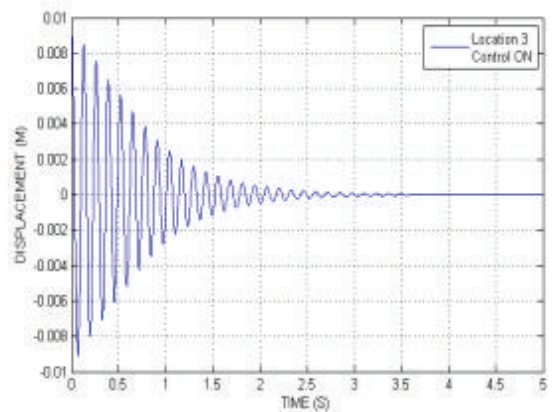


Figure69. Tip displacement Response (K=10)

Table10. Settling Time

Control Gain (k)	Experimental	ANSYS		
	Location 1	Location 1	Location 2	Location 3
0	15s	15s	20s	25s
12	2.5s	1s	Over Damping	
10			2.8s	4s

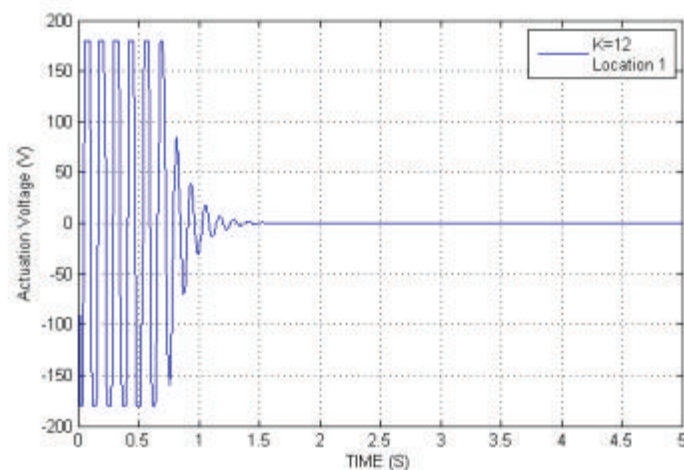


Figure70. Actuation Voltage for controller gain K= 12

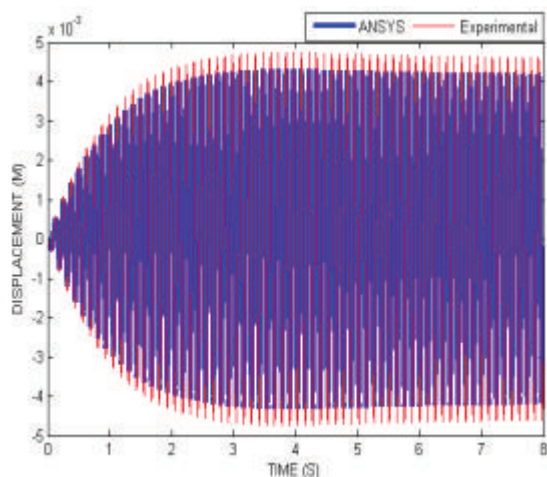


Figure71. Experimental & ANSYS Tip Displacement Response (K=0)

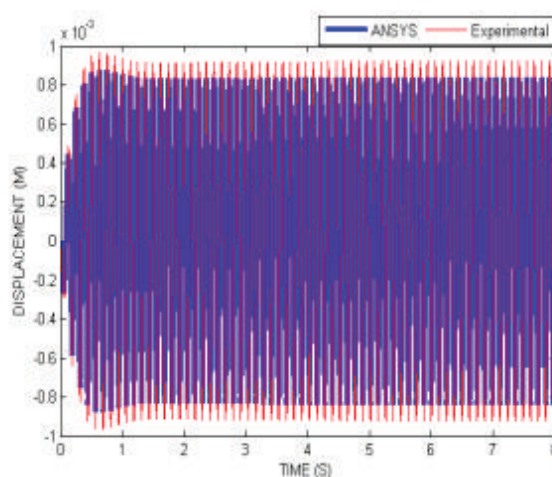


Figure72. Experimental & ANSYS Tip Displacement Response (K=10)

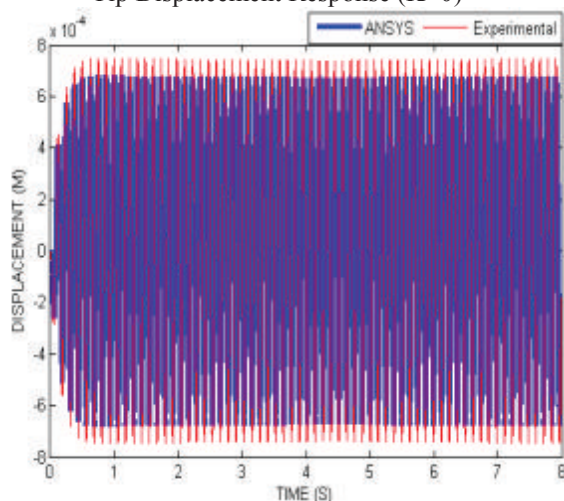


Figure73. Experimental & ANSYS Tip Displacement Response (K=12)

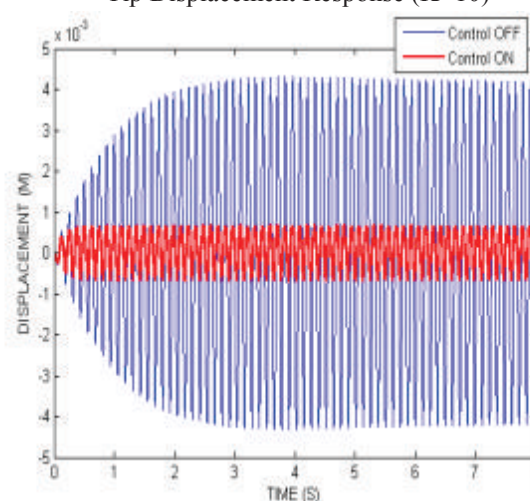
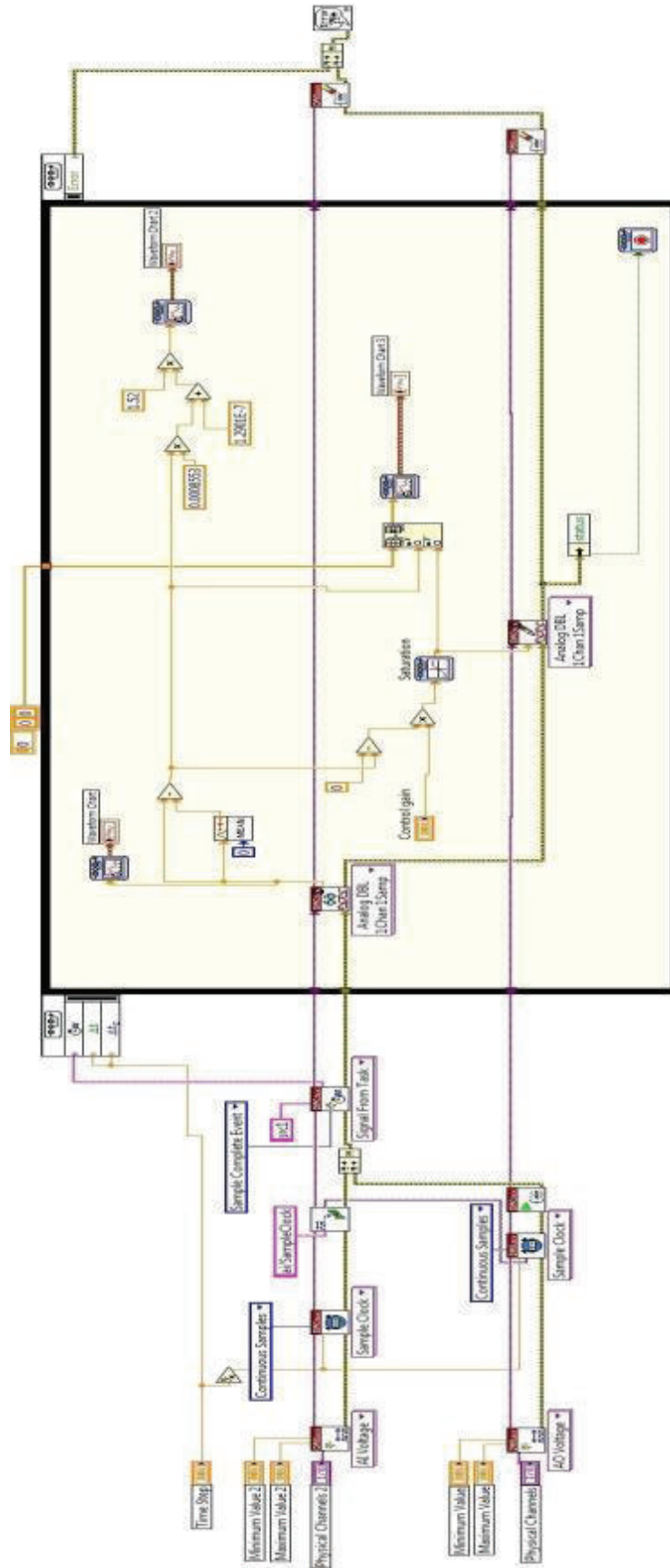


Figure74. Different between Responses for K=0 and K=12

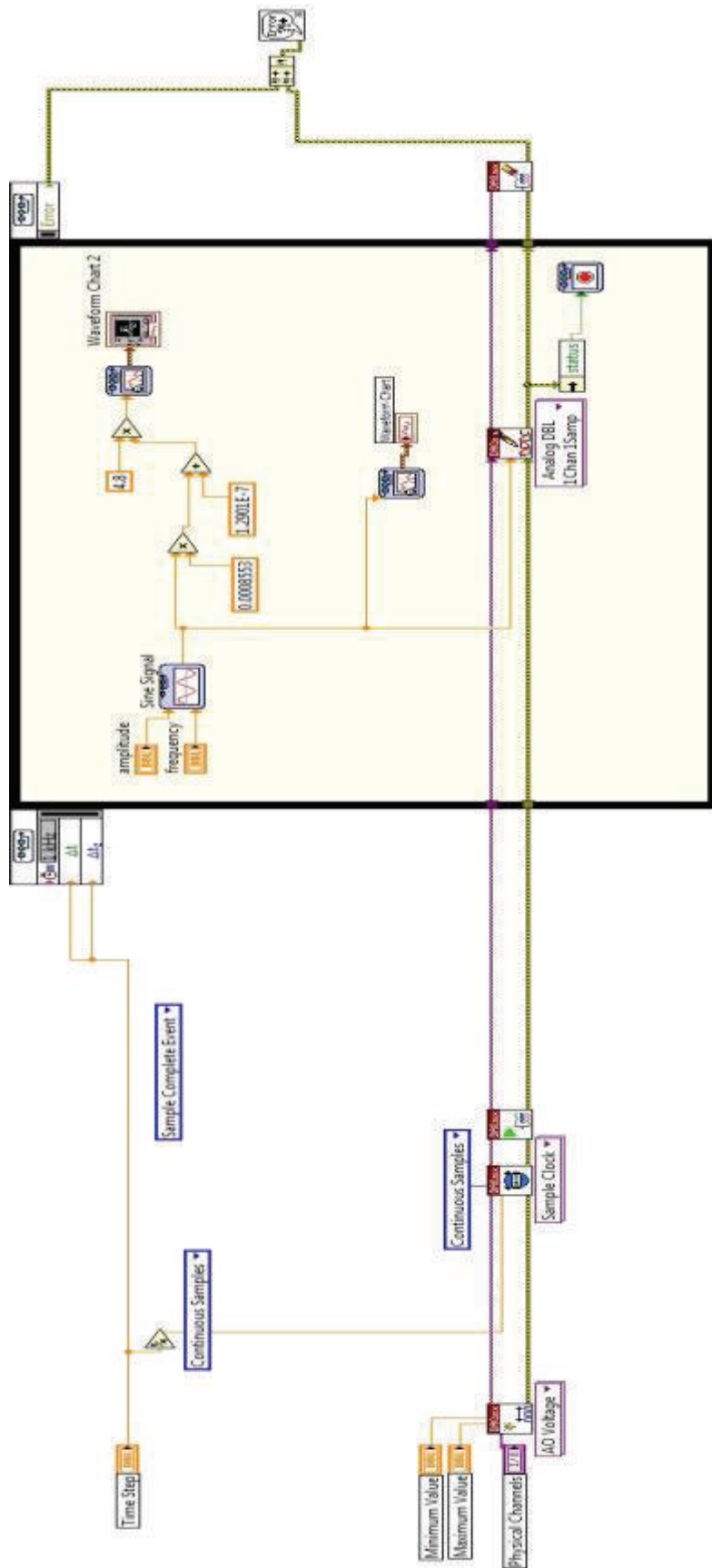
Table11. Amplitude of Tip Displacement

Control Gain (K)	Amplitude (M)	
	Experimental	ANSYS
0	± 0.0046	± 0.0042
10	± 0.00092	± 0.00083
12	± 0.00074	± 0.00067

Appendix (A1)



ACTIVE VIBRATION CONTROL OUTPUT FEEDBACK SYSTEM



Harmonic
Excitation
Sine Wave

The IISTE is a pioneer in the Open-Access hosting service and academic event management. The aim of the firm is Accelerating Global Knowledge Sharing.

More information about the firm can be found on the homepage:

<http://www.iiste.org>

CALL FOR JOURNAL PAPERS

There are more than 30 peer-reviewed academic journals hosted under the hosting platform.

Prospective authors of journals can find the submission instruction on the following page: <http://www.iiste.org/journals/> All the journals articles are available online to the readers all over the world without financial, legal, or technical barriers other than those inseparable from gaining access to the internet itself. Paper version of the journals is also available upon request of readers and authors.

MORE RESOURCES

Book publication information: <http://www.iiste.org/book/>

Academic conference: <http://www.iiste.org/conference/upcoming-conferences-call-for-paper/>

IISTE Knowledge Sharing Partners

EBSCO, Index Copernicus, Ulrich's Periodicals Directory, JournalTOCS, PKP Open Archives Harvester, Bielefeld Academic Search Engine, Elektronische Zeitschriftenbibliothek EZB, Open J-Gate, OCLC WorldCat, Universe Digital Library , NewJour, Google Scholar

